Geochemical Perspectives Letters

Release of subducted sedimentary nitrogen throughout Earth's mantle

P.H. Barry[1,2]*, D.R. Hilton[1]

OPEN ACCESS

Abstract

doi: 10.7185/geochemlet.1615

The dynamic process of subduction represents the principal means to introduce chemical heterogeneities into Earth's interior. In the case of nitrogen (N) - atmosphere's most abundant gas - biological-activity converts N_2 into ammonium ions (NH_4^+), which are chemically-bound within seafloor sediments and altered oceanic crust that comprise the subducting slab. Although some subducted N re-emerges via arc-related volcanism (Sano *et al.*, 1998; Fischer *et al.*, 2002), the majority likely bypasses sub-arc depths (150-200 km) and supplies the deeper mantle (Li *et al.*, 2007; Mitchell *et al.*, 2010; Johnson and Goldblatt, 2015; Bebout *et al.*, 2016). However, the fate of subducted N remains enigmatic: is it incorporated by the shallow convecting mantle - the source of ridge volcanism, or is the deeper mantle - nominally associated with mantle plumes - its ultimate repository? Here, we present N-He-Ne-Ar isotope data for oceanic basalts from the Central Indian Ridge (CIR)-Réunion plume region to address this issue. All on-axis samples with depleted MORB mantle (DMM) affinities ($^3He/^4He$ = 8 ± 1 R_A; Graham, 2002) have low N-isotopes (mean $\delta^{15}N$ = -2.1 ‰), whereas those with plume-like $^3He/^4He$ display higher values (mean $\delta^{15}N$ = 1.3 ‰). We explain these data within the framework of a new mantle reference model to predict a time-integrated net N regassing flux to the mantle of ~3.4 × 10^{10} mol/yr, with the plume-source mantle representing the preferential destination by a factor of 2-3. The model has implications for the present-day imbalance between N subducted at trenches and N emitted via arc-related volcanism, the N-content of Earth's early atmosphere, as well as relationships between N_2 and the noble gases in mantle reservoirs, including $^3He/^4He$-$\delta^{15}N$ relationships in plume-derived lavas.

Received 3 February 2016 | Accepted 11 April 2016 | Published 3 May 2016

Letter

The CIR-Réunion plume system is a classic modern example of oblique plume-ridge interaction, with the present-day plume centred at Réunion Island and three submarine off-ridge segments, the Rodriguez, Three Magi and Gasitao ridges,

1. Fluids & Volatiles Laboratory, Scripps Institution of Oceanography, UC San Diego, La Jolla, California 92093-0244, USA
2. Present address: Department of Earth Sciences, University of Oxford, OX1 3AN, UK

* Corresponding author (email: peter.barry@earth.ox.ac.uk)

connecting with the CIR ridge axis located ~1100 km to the east. These west-to-east trending ridges were formed by volcanism above a channel of Réunion hotspot mantle as the CIR migrated northeast over and away from the plume (Morgan, 1978). He-isotopes – the canonical tracer of mantle plume involvement in petrogenesis – are higher (>9 R_A) than typical DMM values of 8 ± 1 R_A (where R_A = air-like $^3He/^4He$) at Réunion Island and along the off-axis ridges. In contrast, the CIR exhibits DMM-like $^3He/^4He$ values along axis, except at the point where the projection of the submarine ridges meets the ridge axis ~19.9 °S (Füri *et al.*, 2011; Fig. S-1).

New nitrogen isotope and abundance analyses, along with accompanying neon and argon data, of basaltic glasses from the CIR axis between 16.7 °S and 20.6 °S, and from the off-axis ridges to the west of the CIR (Fig. S-1) are presented in Table 1a and b. In addition, we report Ne and Ar isotope and abundance data on olivine separates of a suite of cumulate dunite xenoliths from Réunion Island. Samples were processed by vacuum crushing with released gases analysed using a noble gas mass spectrometer (Barry *et al.*, 2012). All samples have been analysed previously for He isotopes, major/minor and trace element chemistry (Füri *et al.*, 2011).

Nitrogen isotope results are presented in the $\delta^{15}N$ notation (where $\delta^{15}N = ((^{15}N/^{14}N_{sample}/^{15}N/^{14}N_{air})-1) \times 1000$) and plotted against He isotopes in Figure 1a, and displayed in comparison to the $\delta^{15}N$ database of ocean basalts in Figure 1b. We highlight the following key features of the N-isotope results. First, all on-axis samples (with the exception of D9-2; $\delta^{15}N$ = 1.16 ‰) have negative $\delta^{15}N$ values. The highest and lowest values are -0.10 and -3.8 ‰ giving an on-axis $\delta^{15}N$ mean value of -2.1 ± 1.1 ‰ (1σ; n = 7) or -1.7 ± 1.6 ‰ (n = 8 if D9-2 is included). Notably, sample D9-2 has a $^3He/^4He$ ratio (7.25 R_A), which falls in the nominal DMM range (8 ± 1 R_A; Graham, 2002) characteristic of most samples on the CIR ridge-axis (Füri et al., 2011). The only on-axis sample (DR10-1) of the present sample suite with a $^3He/^4He$ value higher than DMM ($^3He/^4He$ = 10.31 R_A) is from the region where the projection of the off-axis ridge impinges the spreading centre (~19.9 °S): it has a $\delta^{15}N$ value of -0.10 ‰ – the second highest value of the on-axis samples. Second, the three off-axis samples – all with $^3He/^4He$ > 9 R_A – have positive $\delta^{15}N$ values, ranging from +0.89 to +1.80 ‰; with a mean value of 1.3 ± 0.7 ‰ (1σ). Thus, with the exception of sample D9-2, there is a clear distinction between relatively low $\delta^{15}N$ values associated with DMM-like He-isotopes on the ridge axis and relatively high $\delta^{15}N$ values associated with plume-like $^3He/^4He$ values off-axis. Finally, we point out that with the exception of sample D8-2, all $\delta^{15}N$ values, irrespective of location on- or off-axis, are higher than the range nominally associated with DMM ($\delta^{15}N$ = -5 ± 2 ‰; Fig. 1b). Thus, samples of this study have experienced enrichment in ^{15}N compared to the majority of basalts erupted at ridge axes worldwide.

There are three processes capable of producing high (>DMM) $\delta^{15}N$ signatures in CIR basalts: (1) assimilation of existing crust during magma eruption, likely also involving incorporation of air ($\delta^{15}N$ = 0 ‰), (2) mass-dependent

Table 1a Neon and argon isotope systematics of submarine basaltic glasses from the CIR (on-axis) and adjacent (off-axis) Gasitao Ridge, Three Magi Ridges and Abyssal Hill, and olivine separates from dunite xenoliths of Piton Chisny (Réunion).

Sample	$^{20}Ne/^{22}Ne$	$^{21}Ne/^{22}Ne$	$^{20}Ne \times 10^{-9}$ cm^3 STP/g	$^{40}Ar/^{36}Ar$	$[^{40}Ar] \times 10^{-9}$ cm^{3}STP/g
On-Axis					
D1-1	10.10 ± 0.11	0.0316 ± 0.0003	0.67 ± 0.012	290.6 ± 0.1	2416 ± 0.3
D1-1 (Dup)	-	-	-	-	-
D3-1	9.90 ± 0.10	0.0291 ± 0.0001	2.28 ± 0.025	296.1 ± 0.3	765 ± 0.5
D2-1	9.85 ± 0.10	0.0295 ± 0.0003	2.21 ± 0.030	349.4 ± 0.3	1415 ± 0.9
D8-2	9.93 ± 0.10	0.0302 ± 0.0002	0.76 ± 0.017	3520 ± 12	724 ± 0.2
D9-2	-	-	-	-	-
D15-1	10.34 ± 0.11	0.0327 ± 0.0004	0.55 ± 0.008	2193 ± 3.3	1968 ± 2.6
D14-1	10.34 ± 0.12	0.0324 ± 0.0008	0.25 ± 0.019	2413 ± 5.8	1326 ± 0.3
D14-1 (Dup)	10.43 ± 0.11	0.0331 ± 0.0004	0.25 ± 0.012	1514 ± 3.9	761 ± 0.7
DR10-1					
D13-1	10.72 ± 0.12	0.0340 ± 0.0006	0.20 ± 0.023	3519 ± 12	722 ± 0.2
D13-1 (Dup)	11.32 ± 0.13	0.0401 ± 0.0007	0.10 ± 0.004	8487 ± 43	1272 ± 0.5
Off-Axis ***Three Magi Ridges***					
D22-1	9.89 ± 0.10	0.0296 ± 0.0002	1.89 ± 0.011	408.5 ± 0.6	1903 ± 0.8
D22-1 (Dup #1)	-	-	-	-	-
D22-1 (Dup #2)	-	-	-	-	-
D26-2	9.87 ± 0.10	0.0296 ± 0.0002	1.15 ± 0.025	554.6 ± 0.5	1268 ± 0.9
Gasitao Ridge					
D20-5	9.84 ± 0.23	0.0294 ± 0.0013	0.17 ± 0.020	1725 ± 12	421 ± 0.1
D20-5 (Dup #1)	10.05 ± 0.13	0.0304 ± 0.0009	0.12 ± 0.007	1786 ± 4.8	383 ± 0.1
D20-5 (Dup #2)	10.05 ± 0.12	0.0317 ± 0.0010	0.14 ± 0.013	1576 ± 5.2	401 ± 0.3
D18-1	9.89 ± 0.11	0.0290 ± 0.0004	0.14 ± 0.006	396.1 ± 3.0	16 ± 0.1
Abyssal Hill					
D37-2	9.86 ± 0.10	0.0294 ± 0.0001	1.19 ± 0.022	318.4 ± 0.4	849 ± 0.7
Réunion Island					
CH07-01	10.49 ± 0.11	0.0306 ± 0.0005	0.30 ± 0.006	1294 ± 3.0	776 ± 0.2
CH07-02	10.00 ± 0.11	0.0296 ± 0.0004	0.33 ± 0.007	501.2 ± 1.0	327 ± 0.2
CH07-04	10.09 ± 0.12	0.0314 ± 0.0014	0.06 ± 0.007	705.1 ± 3.5	125 ± 0.1
CH07-07	10.26 ± 0.11	0.0296 ± 0.0008	0.20 ± 0.006	831.3 ± 2.0	308 ± 0.1

Table 1b Nitrogen and He isotope systematics, and relative He-N-Ar abundances of submarine basaltic glasses from the CIR (on-axis) and adjacent (off-axis) Gasitao Ridge, Three Magi Ridges and Abyssal Hill, and olivine separates from dunite xenoliths of Piton Chisny (Réunion).

Sample	$[N_2] \times 10^{-6}$cm^3 STP/g[a]	$\delta^{15}N$ (‰)[b]	N_2/Ar[c]	$^3He/^4He$ (R/R_A)[d]	$^4He/^{40}Ar^*$
On-Axis					
D1-1	5.56	-1.93 ± 0.91	132	8.11 ± 0.11	-
D1-1 (Dup)	5.21	-1.25 ± 0.71	99.9	-	-
D3-1	4.97	-1.81 ± 1.13	68.5	7.91 ± 0.02	-
D2-1	-	-	-	8.19 ± 0.09	62 ± 0.2
D8-2	21.1	-3.81 ± 0.51	156	7.08 ± 0.14	7.5 ± 0.9
D9-2	10.5	1.16 ± 0.59	267	7.25 ± 0.08	-
D15-1	38.7	-2.34 ± 0.55	281	8.68 ± 0.01	8.4 ± 0.3
D14-1	16.0	-2.01 ± 0.38	238	8.46 ± 0.02	6.9 ± 0.4
D14-1 (Dup)	-	-	-	-	10 ± 0.4
DR10-1	48.0	-0.10 ± 0.63	47.9	10.31 ± 0.06	-
D13-1	20.9	-1.99 ± 0.53	85.6	8.26 ± 0.03	3.0 ± 0.1
D13-1 (Dup)	14.1	-2.68 ± 0.51	131	-	6.0 ± 2.6
Off-Axis ***Three Magi Ridges***					
D22-1	74.2	1.71 ± 0.45	82.8	9.40 ± 0.06	23 ± 0.1
D22-1 (Dup #1)	78.7	1.80 ± 0.52	127	-	-
D22-1 (Dup #2)	92.6	1.74 ± 0.48	104	-	-
D26-2	15.2	0.89 ± 0.83	129	9.51 ± 0.02	5.2 ± 0.1
Gasitao Ridge					
D20-5	-	-	-	8.28 ± 0.05	11 ± 1.3
D20-5 (Dup #1)	-	-	-	-	9.3 ± 0.4
D20-5 (Dup #2)	-	-	-	-	11 ± 0.6
D18-1	2.34	1.14 ± 1.47	244	9.09 ± 0.06	31 ± 0.9
Abyssal Hill					
D37-2	-	-	-	9.67 ± 0.17	18 ± 0.1
Réunion Island					
CH07-01	-	-	-	13.95 ± 0.25	1.3 ± 0.1
CH07-02	-	-	-	13.66 ± 0.22	1.5 ± 0.1
CH07-04	-	-	-	14.09 ± 0.23	2.0 ± 0.1
CH07-07	-	-	-	13.58 ± 0.15	1.5 ± 0.1

[a] N_2 concentration measurements are accurate within 3 %, based on the reproducibility of standards.
[b] Uncertainties on $\delta^{15}N$ are 1σ. Blank subtractions and a comprehensive CO correction have been applied to all $\delta^{15}N$ results.
[c] All N_2/Ar uncertainties are less than 10 %. Blank subtractions have been applied to all N_2/Ar results.
[d] Data previously reported in Füri *et al.*, 2011.

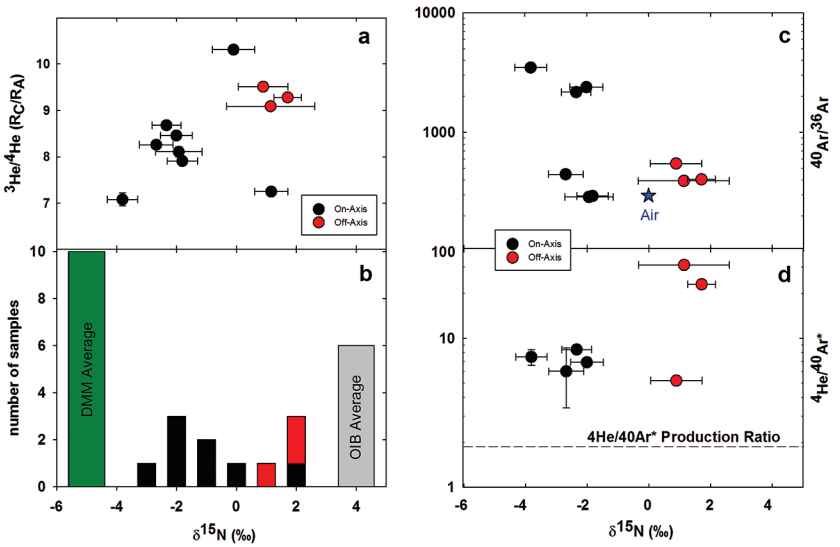

Figure 1 **(a)** He-isotopes (^{3}He/^{4}He) versus N-isotopes, showing high (positive) δ^{15}N values in all off-axis samples with >DMM-like ^{3}He/^{4}He values. **(b)** Histogram of N-isotopes measured along the CIR (in black) and its adjacent ridges (in red) relative to global DMM (green) and OIB (grey) averages (from Cartigny and Marty, 2013). **(c)** Argon isotopes (^{40}Ar/^{36}Ar) versus N-isotopes. **(d)** ^{4}He/^{40}Ar* (degassing proxy) versus N-isotopes suggests that high δ^{15}N values are not produced by magmatic degassing (see text).

fractionation related to magmatic degassing (Cartigny *et al.*, 2001), and/or (3) recycling of oceanic sediments and/or oceanic crust (δ^{15}N ~+5 to +7 ‰) into the CIR mantle source region producing the melts (Marty and Dauphas, 2003). The latter possibility implies that δ^{15}N is a feature intrinsic to the mantle source, whereas the former two are predominantly shallow-level phenomena that act to mask primary (source) δ^{15}N signatures.

There is little evidence in either the on- or off-axis N database (Table 1a and b) for a correlation between high N-contents – possibly reflecting crustal assimilation and/or air addition – and high δ^{15}N values. For example, there is a 30-fold difference in N-content between off-axis samples D22-1 and D18-1 yet they have indistinguishable δ^{15}N values. Similarly, two of the three highest N-content on-axis samples (D8-2 and D15-1) have the lowest δ^{15}N values of this suite. Both observations are inconsistent with addition of air and/or crustal N, which would act to increase both δ^{15}N and N-content of samples. Furthermore, a plot of ^{40}Ar/^{36}Ar versus δ^{15}N (Fig. 1c) shows no correlation for either on- or off-axis samples: all on-axis samples fall within 2σ of the mean value of -2.1 ‰, yet ^{40}Ar/^{36}Ar values range between 8500 and close to the atmospheric value (298.6; Lee *et al.*, 2006), *i.e.* samples with low ^{40}Ar/^{36}Ar values do not have δ^{15}N values closer to air (0 ‰). Finally, off-axis samples are characterised by markedly

different ^{4}He/^{40}Ar* ratios – a parameter sensitive to magma degassing due to the factor of ~10 difference in solubility between He and Ar in basaltic melt (Lux, 1987). Although ^{4}He/^{40}Ar* ratios vary between 5-31 for samples D18-1 and D26-2, respectively, their δ^{15}N values are virtually identical at 1.14 and 0.89 ‰ (Fig. 1d). Thus, we conclude that the range in δ^{15}N values reported here reflects intrinsic mantle source features, likely related to subduction of ^{15}N-enriched oceanic sediments and/or oceanic crust.

The neon isotope characteristics of CIR lavas are plotted on a traditional three-isotope Ne diagram (Fig. S-2). We note that all samples lie intermediate to air-DMM and air-Réunion mixing trajectories with no clear distinction between on- and off-axis samples. Thus, all CIR basalts comprise three Ne components: air, a primitive/solar (mantle) Ne component and in-situ nucleogenic ^{21}Ne, which has in-grown over time. We subtract the air-derived Ne to yield a mantle ^{21}Ne/^{22}Ne ratio (the so-called extrapolated value – (^{21}Ne/^{22}Ne$_{EX}$); see Supplementary Information for details). This approach allows us to assess mantle neon features of both on- and off-axis samples without compromise of air contamination, and to compare Ne isotopes to corresponding N-isotope variations.

In Figure 2, we plot the extrapolated Ne-isotope values (^{21}Ne/^{22}Ne$_{EX}$) of all basalts against measured δ^{15}N together with endmember compositions for (1) pre-solar nitrogen (PSN), (2) depleted MORB mantle (DMM) and (3) sediment-modified mantle (SMM). Pure DMM has a δ^{15}N value of ~-5 ± 2 ‰, which reflects mixing between N incorporated at the time of planetary accretion – small amounts of primordial N (δ^{15}N <-40 ‰), possibly as low as proto-solar-nebula (PSN) nitrogen (δ^{15}N = -383 ± 8 ‰), and nitrogen introduced into the mantle by long-term recycling of atmospheric (= 0 ‰) and/or sediment-derived (= ~+5 to +7 ‰) components (Marty, 2012). SMM nitrogen reflects superimposition and dominance of recently-added sedimentary N relative to pure DMM, as observed at convergent margins such as Costa Rica (Fischer *et al.*, 2002). For Ne-isotopes, a DMM ^{21}Ne/^{22}Ne endmember value (0.0594) is derived by extrapolating the MORB trajectory (Sarda *et al.*, 1988) to the ^{20}Ne/^{22}Ne value of Ne-B (= 12.5) and noting the ^{21}Ne/^{22}Ne value at that point. Solar Ne is defined by the solar wind value of 0.03118 (Trieloff and Kunz, 2005). We assume that subduction of oceanic sediments and crust does not introduce neon (or helium) into the mantle (Hilton *et al.*, 1992) so that DMM and SMM have the same ^{21}Ne/^{22}Ne$_{EX}$ value.

The coupled δ^{15}N-^{21}Ne/^{22}Ne$_{EX}$ characteristics of both sets of basaltic glasses (*i.e.* on- and off-axis) are compatible with mixing between two distinct endmember compositions (Fig. 2). One endmember, with low δ^{15}N and low ^{21}Ne/^{22}Ne$_{EX}$, is common to both sample suites, with solar gas being the most plausible candidate. In contrast, the second endmember differs between on- and off-axis samples. In the case of CIR on-axis basalts, the endmember has a DMM ^{21}Ne/^{22}Ne$_{EX}$ value (0.060) and δ^{15}N = -2.1 ‰ whereas the off-axis samples project to an endmember with a higher δ^{15}N (~1.3 ‰) but the same DMM-like ^{21}Ne/^{22}Ne$_{EX}$ value. Notably, both on- and off-axis endmembers lie on the projection between pure DMM and SMM with the proportion of N derived from SMM clearly greater in off-axis samples versus on-axis samples (Fig. 2).

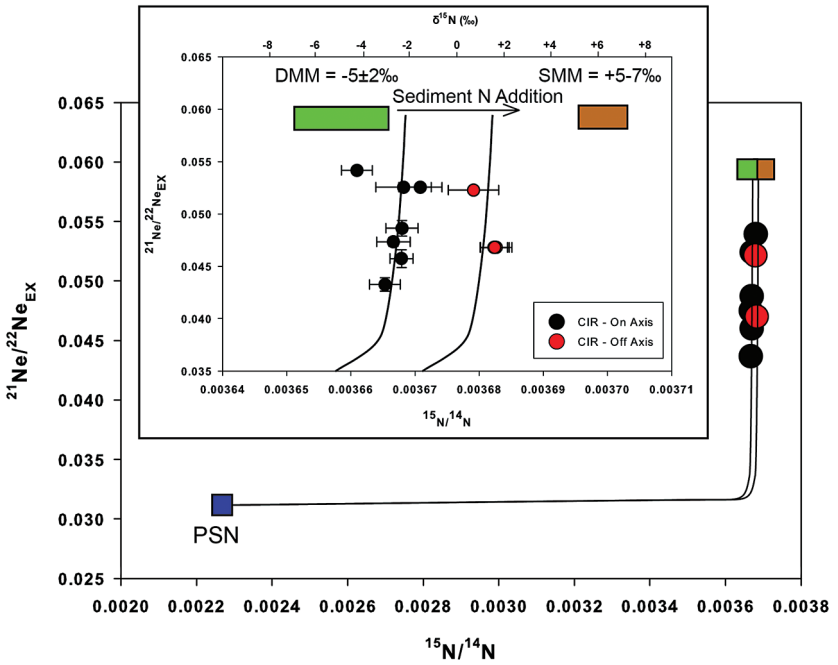

Figure 2 Extrapolated Ne ($(^{21}Ne/^{22}Ne)_{EX}$, *i.e.* air-corrected $^{21}Ne/^{22}Ne$ values) versus $^{15}N/^{14}N$ values of CIR basalts, plotted together with binary mixing curves between a pre-solar nitrogen (PSN) component ($^{15}N/^{14}N$ = 0.00227, $\delta^{15}N$ = -373 ‰; Marty, 2012) and two mantle endmember components reflecting addition of ^{15}N-enriched sedimentary MORB mantle (SMM; $\delta^{15}N$ = +5 ‰) to DMM mantle ($\delta^{15}N$ = -5 ‰). The curvature of the hyperbolic mixing lines is described by the r-value = $(^{14}N/^{22}Ne)_{DMM/SMM}/(^{14}N/^{22}Ne)_{PSN}$.

The curvature of the binary mixing trajectories in Figure 2 has important implications for the overall recycling efficiency of N relative to Ne, as it is controlled by the relative $^{14}N/^{22}Ne$ ratios of the two endmembers (r-value). For both on- and off-axis samples, r ≥ 1000, which indicates either higher relative ^{14}N or lower ^{22}Ne contents in the mixed DMM-SMM versus the PSN endmember: this indicates that N is recycled at least 10^3 times more efficiently than Ne into the CIR mantle. Preferential deep recycling of N relative to Ne is consistent with recent theoretical and experimental predictions that indicate that N is stabilised as ammonium under subduction redox conditions (fO_2 < QFM; Mikhail and Sverjensky, 2014) and therefore behaves as a large ion lithophile element whereby it can substitute into K-bearing silicate minerals and gain stability in the downgoing slab (Li *et al.*, 2013). Moreover, mass balance arguments suggest Ne is efficiently recycled back to the surface during the subduction process (Holland and Ballentine, 2006; Marty, 2012).

The CIR data reaffirms the considerable heterogeneity in mantle $\delta^{15}N$ signatures (*e.g.*, Marty and Dauphas, 2003). If we assume that on-axis samples can be used to approximate the N composition of the DMM and that off-axis samples best represent the plume mantle (PLM), then CIR data can be used within the framework of a newly-constructed reference model to place constraints on N regassing fluxes into the mantle (*i.e.* both absolute flux values as well as the relative proportions regassing the DMM and PLM reservoirs). Our model is based on a layered mantle reservoir concept, similar to that described for noble gases by O'Nions and Tolstikhin (1996) and Gonnermann and Mukhopadhyay (2009). It makes the following assumptions: (1) the N regassing flux commences at the onset of subduction and is constant through time; (2) a constant proportion of the total N regassing flux (F) is subducted into each respective mantle reservoir (defined here as F_{DMM} and F_{PLM}) and instantaneously mixes in each reservoir; (3) there is a constant mantle degassing flux of 5×10^9 mol/yr (Cartigny and Marty, 2013), derived from the DMM:PLM reservoirs in the proportion 85:15, respectively (Ito *et al.*, 2003); (4) the present-day mantle N-content ([N]) is ~0.27 ± 0.16 ppm (Marty, 2012; Cartigny and Marty, 2013); and (5) the initial mantle $\delta^{15}N$ is -40 ‰ (PSN-like; Cartigny and Marty, 2013) which is unmodified by any degassing prior to the onset of subduction. The DMM and PLM reservoirs are considered to have evolved to their current $\delta^{15}N$ and [N] compositions, given by the CIR data, as a consequence of additions of different amounts of subducted sedimentary N ($\delta^{15}N$ = +5 ‰).

A DMM mass of ~9×10^{26} g (*e.g.*, Anderson, 1989) corresponds to a total inventory of 17.3×10^{18} mol N in the modern-day DMM. Assuming that the mantle degassing flux (5×10^9 mol/yr; Cartigny and Marty, 2013) includes all non-arc related N (*i.e.* N degassed from the mantle) and is 85 % DMM-derived (4.3×10^9 mol/yr) and 15 % plume mantle-derived (7.5×10^8 mol/yr), then a total of 10.6×10^{18} mol N has been degassed from the DMM source over an estimated 2.5 Ga since subduction commenced (*e.g.*, Kusky *et al.*, 2001). For a total N-content of 27.9×10^{18} mol N before degassing, the present-day N-isotopic composition of -2.1 ‰ must represent admixture between 23.5×10^{18} moles of subduction-derived N ($\delta^{15}N$ = +5 ‰), or ~84 % of the total N, and 4.4×10^{18} moles (or 16 %) of PSN ($\delta^{15}N$ = -40 ‰). Thus, the time integrated DMM regassing rate (F_{DMM}) is 9.4 x 10^9 moles/yr.

Using the same approach for the PLM – assumed to be represented by off-axis high $^3He/^4He$ plume melts with an average $\delta^{15}N$ = 1.3 ‰, then a mass of ~3.3×10^{27} g would contain 64×10^{18} mol N in the modern day plume-influenced mantle. Again assuming a constant mantle degassing flux of 5×10^9 mol/yr (Cartigny and Marty, 2013), of which ~15 % (*i.e.* 7.5×10^8 mol/yr) is derived from this reservoir (Ito *et al.*, 2003), then a total of 1.9×10^{18} mol N has been degassed from the plume-influenced mantle over 2.5 Ga. The total N-content of 65.9×10^{18} mol requires 61×10^{18} moles N (~92 % of the total) of subduction-derived N ($\delta^{15}N$ = +5 ‰) mixing with 8 % (*i.e.* 5.4×10^{18} moles) of PSN ($\delta^{15}N$ = -40 ‰) to give the present-day N-isotopic composition of 1.3 ‰. Thus, the model predicts a regassing N-flux (F_{PLM}) of ~2.4×10^{10} mol/yr since the Archean (2.5 Ga). Importantly,

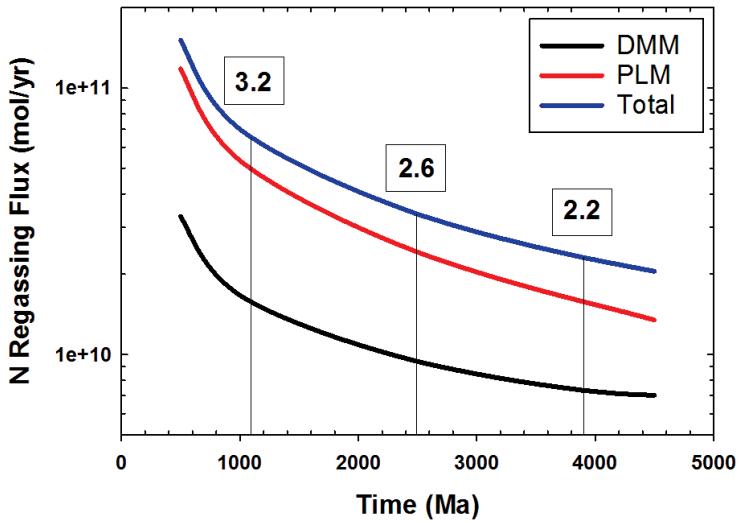

Figure 3 Nitrogen regassing fluxes (mol/yr) into the mantle as a function of time (Ma) since the onset of subduction. The total flux is equal to the sum of DMM and PLM fluxes. The proportion of N regassed into the plume-influenced mantle relative to the DMM (F_{PLM}/F_{DMM}) is shown in boxes at three given time intervals (1.1 Ga, 2.5 Ga, 3.9 Ga).

in order to satisfy the N systematics for both reservoirs, approximately 2.6 times more N (*i.e.* F_{PLM}/F_{DMM}) must be subducted into the plume-influenced mantle. If subduction is assumed to have initiated earlier in the geological record (*e.g.*, 3.9 Ga; Condie and Pease, 2008), then the F_{PLM}/F_{DMM} ratio decreases to ~2.2. Conversely, if an estimated modern day N input flux of 7×10^{10} mol/yr (Cartigny and Marty, 2013) is adopted, it would take the Earth only 1.1 Ga to evolve to its current N composition, with $F_{PLM}/F_{DMM} = 3.2$ (Fig. 3; Table S-1).

Selection of different $\delta^{15}N$ endmembers for mantle reservoirs or lower initial solar values as input parameters has only a minor effect on model results (Table S-1). If more extreme N-isotope estimates of -4 ‰ and +3 ‰ are taken to approximate DMM and PLM sources, respectively (Dauphas and Marty, 1999), then an identical PLM regassing flux of 2.4×10^{10} mol/yr is calculated for 2.5 Ga with only a marginally higher $F_{PLM}/F_{DMM} = 2.8$. Alternatively, a significantly higher estimate for the mantle N-content of ~36 ppm (Cartigny and Marty, 2013) results in a 2.5 Ga regassing flux of 3.9×10^{12} mol/yr with a $F_{PLM}/F_{DMM} = 4$. Significantly, all model scenarios point to long-term cycling of subducted N into Earth's mantle with preferential storage in the deep (plume) mantle (*i.e.* $F_{PLM}/F_{DMM} > 2$). Thus nitrogen not only breaches the subduction barrier beneath arcs but is also transported into the (deep mantle) source region that supplies high $^3He/^4He$ mantle plumes.

Our new reference model has a number of far-reaching implications. First, given the high N recycling efficiencies into DMM (84 %) and PLM (92 %) reservoirs, respectively (this work), any losses of slab-derived N to the atmosphere at volcanic arcs (*e.g.*, by oxidation back to molecular form in the mantle wedge) must be relatively minor. Thus, our model can explain the present-day gross imbalance between the regassing N flux subducted via trenches and the degassing N flux returned to the surface via arc-related volcanism (Hilton *et al.*, 2002; Busigny *et al.*, 2011). Second, prior to initiation of subduction-related recycling of N, the total N content of the atmosphere must have been considerably higher. Our model indicates that the early atmospheric N content was ~2.1 x 10^{20} moles, or ~50 % higher than at the present-day. Such a high atmospheric N-content would lead to N-enhanced greenhouse warming, and can explain the lack of global glaciations in the early Earth due to the faint young Sun (Goldblatt *et al.*, 2009). Third, subduction of sedimentary N into the deep mantle would lead to a close relationship between high $\delta^{15}N$ values and high $^3He/^4He$ ratios, the canonical geochemical tracer of deep mantle plumes. Recent work on hyaloclastic basaltic glasses in Iceland (Halldórsson *et al.*, 2016) reveals a strong coupling between $^3He/^4He$ and $\delta^{15}N$ signatures, consistent with recycling of crustal material to the mantle plume source. Finally, we highlight remarkably similar recycling efficiencies between N (84-92 %; this work) and heavy noble gases (73-87 %; Holland and Ballentine, 2006; Parai and Mukhopadhyay, 2012) despite fundamentally different subduction mechanisms: N is fixed as NH_4^+ and bound in recycled sediments and/or oceanic crust, whereas Kr and Xe undergo no such chemical transformation and instead are simply dissolved in pore fluids and/or in unoccupied amphibole A-sites within subducted oceanic crust (*e.g.*, Holland and Ballentine, 2006; Jackson *et al.*, 2015).

Acknowledgements

This work was supported by NSF grants EAR-0651097 and OCE-0726573. The KNOX11RR cruise was funded by UC Ship Funds. We thank Sami Mikhail, Ben Johnson and anonymous reviewers for their constructive and insightful comments, and Graham Pearson for editorial handling.

Editor: Graham Pearson

Additional Information

Supplementary Information accompanies this letter at www.geochemicalperspectivesletters.org/article1615

Reprints and permission information is available online at http://www.geochemicalperspectivesletters.org/copyright-and-permissions

Cite this letter as: Barry, P.H., Hilton, D.R. (2016) Release of subducted sedimentary nitrogen throughout Earth's mantle. *Geochem. Persp. Let.* 2, 148-159.

References

Anderson, D.L. (1989) Theory of the Earth. Blackwell Scientific Publications, Boston, http://resolver.caltech.edu/CaltechBOOK:1989.001.

Barry, P.H., Hilton, D.R., Halldórsson, S.A., Hahm, D., Marti, K. (2012) High precision nitrogen isotope measurements in oceanic basalts using a static triple collection noble gas mass spectrometer. *Geochemistry Geophysics Geosystems* 13, Q01019.

Bebout, G.E., Lazzeri, K.E., Geiger, C.A. (2016) Pathways for nitrogen cycling in Earth's crust and upper mantle: A review and new results for microporous beryl and cordierite. *American Mineralogist* 101, 7-24.

Busigny, V., Cartigny, P., Philippot, P. (2011) Nitrogen isotopes in ophiolitic metagabbros: A re-evaluation of modern nitrogen fluxes in subduction zones and implication for the early Earth atmosphere. *Geochimica et Cosmochimica Acta* 75, 7502–7521.

Cartigny, P., Marty, B. (2013) Nitrogen isotopes and mantle geodynamics: The emergence of life and the atmosphere–crust–mantle connection. *Elements* 9, 359-366.

Cartigny, P., Harris, J.W., Javoy, M. (2001) Diamond genesis, mantle fractionations and mantle nitrogen content: a study of δ13 C–N concentrations in diamonds. *Earth and Planetary Science Letters* 185, 85-98.

Condie, K.C., Pease, V. (2008) When did plate tectonics begin on planet Earth? Geological Society of America Special Paper 440, Boulder Colorado, USA.

Dauphas, N., Marty, B. (1999) Heavy nitrogen in carbonatites of the Kola Peninsula: A possible signature of the deep mantle. *Science* 286, 2488-2490.

Fischer, T.P., Hilton, D.R., Zimmer, M.M., Shaw, A.M., Sharp, Z.D., Walker, J.A. (2002) Subduction and recycling of nitrogen along the Central American margin. *Science* 297, 1154-1157.

Füri, E., Hilton, D.R., Murton, B.J., Hemond, C., Dyment, J., Day, J.M.D. (2011) Helium isotope variations between Réunion Island and the Central Indian Ridge (17°-21°S): new evidence for ridge-hotspot interaction. *Journal of Geophysical Research – Solid Earth* 116, B02207.

Graham, D.W. (2002) Noble gas isotope geochemistry of mid-ocean ridge and ocean island basalts: Characterization of mantle source reservoirs. *RIMS* 47, 247-317.

Goldblatt, C., Claire, M.W., Lenton, T.M., Matthews, A.J., Watson, A.J., Zahnle, K.J. (2009) Nitrogen-enhanced greenhouse warming on early Earth. *Nature Geoscience* 2, 891-896.

Gonnermann, H.M., Mukhopadhyay, S. (2009) Preserving noble gases in a convecting mantle. *Nature* 459, 560-563.

Halldórsson, S.A., Hilton, D.R., Barry, P.H., Füri, E., Gronvold, K. (2016) Recycling of crustal material by the Iceland mantle plume: New evidence from nitrogen elemental and isotope systematics of subglacial basalts. *Geochimica et Cosmochimica Acta* 176, 206-226.

Hilton, D.R., Hoogewerff, J.A., Van Bergen, M.J., Hammerschmidt, K. (1992) Mapping magma sources in the east Sunda-Banda arcs, Indonesia: constraints from helium isotopes. *Geochimica et Cosmochimica Acta* 56, 851-859.

Hilton, D.R., Fischer, T.P., Marty, B. (2002) Noble gases and volatile recycling at subduction zones. *Reviews in Mineralogy and Geochemistry* 47, 319-370.

Holland, G., Ballentine, C.J. (2006) Seawater subduction controls the heavy noble gas composition of the mantle. *Nature* 441, 186-191.

Ito, G., Lin, J., Graham, D. (2003) Observational and theoretical studies of the dynamics of mantle plume–mid-ocean ridge interaction. *Reviews of Geophysics* 41, 4.

Jackson, C.R., Parman, S.W., Kelley, S.P., Cooper, R.F. (2015) Light noble gas dissolution into ring structure-bearing materials and lattice influences on noble gas recycling. *Geochimica et Cosmochimica Acta* 159, 1-15.

Johnson, B., Goldblatt, C. (2015) The nitrogen budget of Earth. *Earth-Science Reviews* 148, 150-173.

Kusky, T.M., Li, J.H., Tucker, R.D. (2001) The Archean Dongwanzi ophiolite complex, North China Craton: 2.505-billion-year-old oceanic crust and mantle. *Science* 292, 1142-1145.

Lee, J.Y., Marti, K., Severinghaus, J.P., Kawamura, K., Yoo, H.S., Lee, J.B., Kim, J.S. (2006) A redetermination of the isotopic abundances of atmospheric Ar. *Geochimica et Cosmochimica Acta* 70, 4507-4512.

Li, L., Bebout, G.E., Idleman, B.D. (2007) Nitrogen concentration and δ 15 N of altered oceanic crust obtained on ODP Legs 129 and 185: insights into alteration-related nitrogen enrichment and the nitrogen subduction budget. *Geochimica et Cosmochimica Acta* 71, 2344-2360.

Li, Y., Wiedenbeck, M., Shcheka, S., Keppler, H. (2013) Nitrogen solubility in upper mantle minerals. *Earth and Planetary Science Letters* 377, 311-323.

Lux, G. (1987) The behavior of noble gases in silicate liquids: Solution, diffusion, bubbles and surface effects, with applications to natural samples. *Geochimica et Cosmochimica Acta* 51, 1549-1560.

Marty, B. (2012) The origins and concentrations of water, carbon, nitrogen and noble gases on Earth. *Earth and Planetary Science Letters* 313-314, 56-66.

Marty, B., Dauphas, N. (2003) The nitrogen record of crust-mantle interaction and mantle convection from Archean to present. *Earth and Planetary Science Letters* 206, 397– 410.

Mikhail, S., Sverjensky, D.A. (2014) Nitrogen speciation in upper mantle fluids and the origin of Earth's nitrogen-rich atmosphere. *Nature Geoscience* 7, 816-819.

Mitchell, E.C., Fischer, T.P., Hilton, D.R., Hauri, E.H., Shaw, A.M., De Moor, J.M., Sharp, Z.D., Kazahaya, K. (2010) Nitrogen sources and recycling at subduction zones: Insights from the Izu-Bonin-Mariana arc. Geochemistry, Geophysics, Geosystems 11, 2.

Morgan, W.J. (1978) Rodriguez, Darwin, Amsterdam, a second type of hot spot island. *Journal of Geophysical Research* 83, 5355–5360.

O'Nions, R.K., Tolstikhin, I.N. (1996) Limits on the mass flux between lower and upper mantle and stability of layering. *Earth and Planetary Science Letters* 139, 213-222.

Parai, R., Mukhopadhyay, S. (2012) How large is the subducted water flux? New constraints on mantle regassing rates. *Earth and Planetary Science Letters* 317, 396-406.

Sano, Y., Takahata, N., Nishio, Y., Marty, B. (1998) Nitrogen recycling in subduction zones. *Geophysical Research Letters* 25, 2289-2292.

Sarda, P., Staudacher, T., Allègre, C.J. (1988) Neon isotopes in submarine basalts. *Earth and Planetary Science Letters* 91, 73–88.

Trieloff, M., Kunz, J. (2005) Isotope systematics of noble gases in the Earth's mantle: possible sources of primordial isotopes and implications for mantle structure. *Physics of the Earth and Planetary Interiors* 148, 13-38.

Release of subducted sedimentary nitrogen throughout Earth's mantle

P.H. Barry[1,2]*, D.R. Hilton[1]

Supplementary Information

The Supplementary Information includes:

- Additional Information and Methods
- Figures S-1 to S-5
- Table S-1
- Supplementary Information References

Additional Information and Methods

Geochemical Tracers of Volatile Recycling into Earth's Mantle

Noble gases are powerful tracers of mantle processes, and sensitive indicators of crustal/sediment inputs to the mantle due to the large isotopic contrast of noble gases between mantle and crustal/atmospheric reservoirs. Light noble gases (helium and neon) in Earth's mantle preserve distinct solar-like isotopic compositions, whereas heavy noble gases (argon, krypton and xenon) display values which are intermediate between solar-like and air-dominated isotopic compositions (Holland and Ballentine, 2006). Surficial helium is not recycled into the mantle during subduction as it is not gravitationally bound to Earth. The fate of Ne is debated (Sarda, 2004): however, due to its relatively low abundance in subducted material, subducted contributions are generally considered negligible (Holland and Ballentine, 2006). Heavier noble gas compositions in the mantle were long considered to be independent of subduction as they were believed to be returned back into the atmosphere through subduction volcanism before they could be admixed into the mantle (Staudacher and Allègre, 1988; Hilton

1. Fluids & Volatiles Laboratory, Scripps Institution of Oceanography, UC San Diego, La Jolla, California 92093-0244, USA
2. Present address: Department of Earth Sciences, University of Oxford, OX1 3AN, UK
* Corresponding author (email: peter.barry@earth.ox.ac.uk)

et al., 2002). This led to the hypothesis that Earth's mantle is insulated from atmospheric heavy noble gas inputs due to an efficient 'subduction barrier' for volatiles. However, recent studies suggest that air-like values in the deep mantle may be the direct result of subduction (Nagao and Takahashi, 1993; Sarda *et al.*, 1988; Matsumoto *et al.*, 2001; Sarda, 2004; Holland and Ballentine, 2006; Sumino *et al.*, 2010; Hopp and Ionov, 2011; Kendrick *et al.*, 2011; Mukhopadhyay, 2012; Parai *et al.*, 2012; Tucker *et al.*, 2012; Kendrick *et al.*, 2013; Jackson *et al.*, 2013a;b; Pető *et al.*, 2013; Jackson *et al.*, 2015; Parai and Mukhopadhyay, 2015; Jackson *et al.*, 2016), thus potentially providing an additional mechanism for monitoring recycling (Honda and Woodhead, 2005; Sumino *et al.*, 2010).

The large isotopic contrast between terrestrial nitrogen reservoirs makes N a potentially powerful tracer of volatile recycling between the surface and mantle (Li *et al.*, 2007; Mitchell *et al.*, 2010; Johnson and Goldblatt, 2015; Bebout *et al.*, 2016). For example, the depleted MORB mantle (DMM) has a lower $^{15}N/^{14}N$ ratio (by -5 ± 2 ‰) than Earth's atmosphere (Javoy *et al.*, 1986; Cartigny *et al.*, 1998; Marty and Zimmermann, 1999; Marty and Dauphas, 2003; Cartigny and Marty, 2013; Palot *et al.*, 2012; Johnson and Goldblatt, 2015; this study). This isotopic contrast was likely established early in Earth's history, reflecting the integrated effects of mantle degassing, late heavy bombardment, and/or hydrodynamic escape of Earth's primary atmosphere (Marty, 2012). Nitrogen is stable as ammonium under subduction redox conditions (fO_2 < QFM; Watenphul *et al.*, 2010; Li *et al.*, 2013; Li and Keppler, 2014; Mikhail and Sverjensky, 2014) and acts much like a large ion lithophile element, substituting for K-bearing minerals and sedimentary material. Subsequent modifications to mantle N may result from subduction of this material comprised of isotopically distinct N (~+5‰) (Sano *et al.*, 1998; Busigny *et al.*, 2013; Thomazo and Papineau, 2013; Halama *et al.*, 2014). For example, modern oceanic sediments are enriched in the heavy isotope of nitrogen (*i.e.* ^{15}N) relative to the DMM. As a result, subduction of altered oceanic crust and sediments, containing molecularly-bound nitrogen – residual to sub-arc fluid loss – could result in the introduction of high N-isotope signatures into the (deep) mantle (Hofmann and White, 1982; Marty and Humbert, 1997; Halama *et al.*, 2010). N-isotope enrichments have been observed in subduction-related geothermal gases (Fischer *et al.*, 2002) and ocean island basalts (OIBs; Hoffman and White, 1982; Mohapatra and Murty, 2002; Marty and Dauphas, 2003; Fischer *et al.*, 2005). To date, however, such N-isotope anomalies have rarely been detected in the DMM (Marty and Zimmermann, 1999; Cartigny *et al.*, 2001).

Geological Setting

The CIR separates the African and Indo-Australian plates and extends over ~3000 km from the Carlsberg Ridge (3.0 °N, 66.0 °E) southwards towards the Rodrigues Triple Junction (20.5 °S, 70.0 °E), where it bifurcates into the Southeast and the Southwest Indian ridges. Basalt samples of this study were collected along a segment of the CIR between 16.7 °S and 20.6 °S, located to the north and south of the Marie Celeste Fracture Zone (FZ) and northwest of the Egeria FZ, respectively

(Fig. S-1). The CIR axis shoals from north to south along this segment. In addition, several off-axis samples were collected along a perpendicularly offset lineament, which extends westward from 66 °E to 64 °E toward the Mascarene Islands (*e.g.*, Réunion, Mauritius, Rodrigues islands; Parson *et al.*, 1993).

During the past ~70 Ma, the Réunion hot spot formed the Deccan Trap flood basalts, the Chagos-Maldive-Laccadive Ridge, the Mascarene Plateau and the Mascarene Islands (Duncan *et al.*, 1989, 1990). At ~34 Ma, the northeastward migrating CIR moved over the Réunion hot spot (Duncan *et al.*, 1990) and embedded a "fossil" Réunion hot spot mantle component into the sub-ridge mantle. The Réunion hot spot is currently located ~1100 km west of the CIR axis (Fig. S-1; Mahoney *et al.*, 1989; Murton *et al.*, 2005). Using He isotopes ratios ($^3He/^4He$) – the canonical tracer of mantle plume involvement in petrogenesis (Courtillot *et al.*, 2003) – Füri *et al.* (2011) identified plume material flowing eastward toward the CIR on a trajectory that impinges the ridge at ~19.9 °S. Réunion Island is composed of two volcanoes: Piton des Neiges, which was active between ~2 Ma and 43 ka, and the currently active Piton de la Fournaise, where volcanic activity began ~530 ka ago (Gillot and Nativel, 1989). The island of Mauritius is located 250 km east of Réunion Island and 850 km west of the CIR, at the previous site of the Réunion hot spot (~8 Ma) (Morgan, 1981; Paul *et al.*, 2005). Rodrigues Island is located ~600 km east of Mauritius and formed at 1.5 Ma (McDougall *et al.*, 1965); it marks the eastern extent of the Rodrigues Ridge, an east-west trending volcanic ridge that is between 8 to 10 Ma old (Duncan *et al.*, 1990). Smaller en-échelon volcanic ridges at 19 °S (*e.g.*, the Three Magi Ridges and the Gasitao Ridge) extend the Rodrigues Ridge close to the CIR (Fig. S-1) (Dyment *et al.*, 1999, 2000). Various models have been proposed to explain the occurrence of volcanism between the Mascarene Islands and the CIR. First, Morgan (1978) proposed that the Rodrigues Ridge was formed by volcanism above a channel of upwelling Réunion hot spot mantle, which was deflected toward the CIR as it migrated northeastward away from the hot spot, and predicted a Réunion signature would be present at the intersection of the CIR with a line projected through Réunion and Rodrigues islands. Mahoney *et al.* (1989) later detected this Réunion-like isotope signature (low $^{143}Nd/^{144}Nd$, high $^{87}Sr/^{86}Sr$, high $^{207}Pb/^{204}Pb$, and high $^{206}Pb/^{204}Pb$) in basalts from the Marie Celeste FZ portion of the CIR.

Several detailed geochemical studies have focused on plume-ridge interaction in the region between the Rodrigues Triple Junction and the Marie Celeste fracture zone. Murton *et al.* (2005) conducted a detailed study of this area and reported enrichments in incompatible elements that increased northward, which they interpreted to reflect the presence of enriched mantle originating at the Réunion hot spot, which had subsequently migrated eastward toward the CIR against the direction of motion of the lithosphere. Nauret *et al.* (2006) also targeted a suite of basalts collected both on and off the CIR axis between 18 °S and 20 °S for Sr-Nd-Pb isotopes and showed that the most trace element enriched samples display the most radiogenic Pb isotopic compositions. Furthermore, they compared basalt samples with submarine Réunion lavas (Fretzdorff

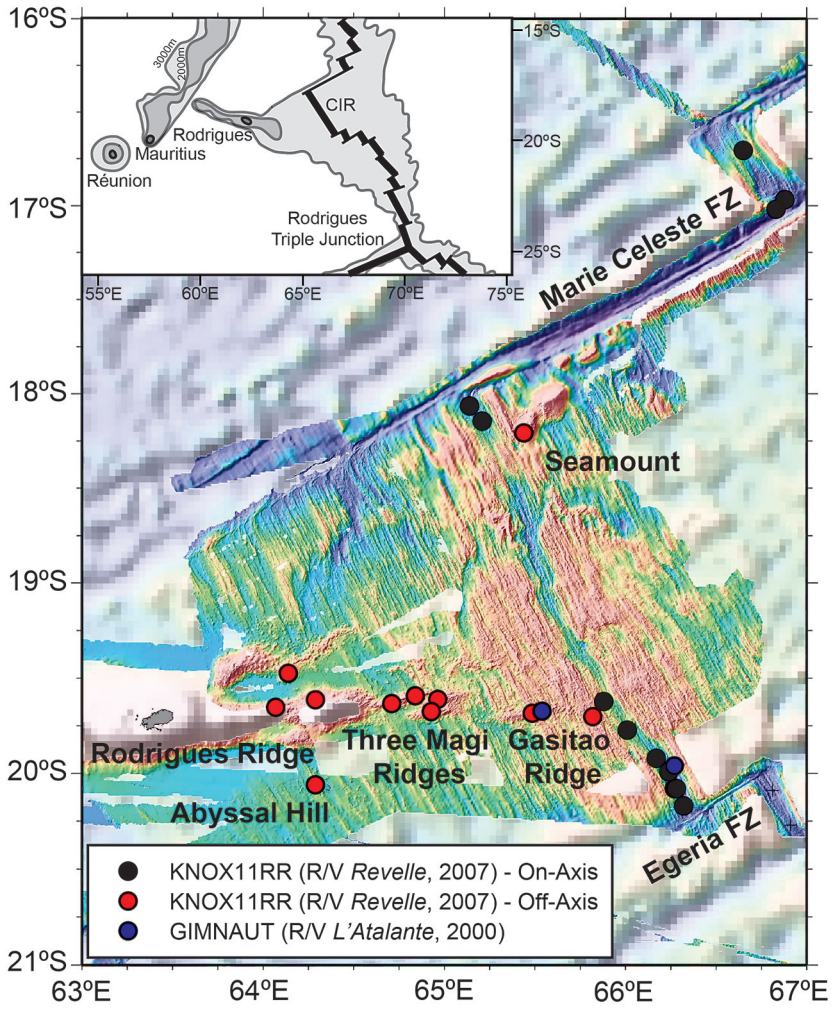

Figure S-1 Bathymetric map of the (on-axis) CIR and the adjacent (off-axis) Gasitao Ridge, Three Magi Ridges, Rodrigues Ridge and Abyssal Hill. Three shades of colours represent bathymetry data: (1) pale colours are bathymetry "predicted" from satellite altimetry (Smith and Sandwell, 1997); (2) intermediate colours represent previous multi-beam bathymetric data from R/V Marion Dufresne (Dyment *et al.*, 1999), R/V L'Atalante (Dyment *et al.*, 2000), and R/V Hakuho-Maru (Okino *et al.*, 2008); (3) bright colours are multibeam bathymetric data collected by R/V Revelle in 2007 (Füri *et al.*, 2008; Füri *et al.*, 2011). The circles indicate the location of samples collected during the KNOX11RR (black = CIR on-axis; red = off-axis) and GIMNAUT (blue) cruises. The inset shows the Mascarene Islands (*i.e.* Réunion, Mauritius, and Rodrigues islands) to the west and the Rodrigues Triple Junction. Map modified from Füri *et al.*, 2011.

and Haase, 2002) and concluded that the radiogenic isotope characteristics of the majority of on-axis samples cannot be explained with a Réunion-like endmember. Recently, however, Ulrich *et al.* (2012) showed that trace element and isotopic enrichments in the 18 °S to 20 °S region of the CIR are consistent with a binary mixture between the regional depleted MORB mantle (DMM) source and a recycled Ocean Iceland Basalt (OIB)/plume component. In contrast, off-axis basalts from the Gasitao Ridge, as well as a single on-ridge sample collected at ~19.9 °S, appeared to record a Réunion source signature. As a result, these authors proposed that Réunion hot spot material flows eastward toward the CIR on a trajectory that impinges the ridge at ~19.9 °S, in agreement with the initial hypothesis put forth by Morgan (1978). Furthermore, they concluded that mantle source enrichment in the vicinity of the Marie Celeste FZ, ~100 km to the north, cannot be related to influx of mantle material from Réunion. Füri *et al.* (2011), however, suggested that these enrichments, along with slightly radiogenic He-isotope values could result from a "fossil" Réunion plume component in the region. In addition, these authors showed that the highest $^{3}He/^{4}He$ values (~12.2 R_A) were measured in glasses from off-axis portions of the CIR, and are consistent with flow of hot spot mantle material from Réunion (~100 km to the west) toward the CIR.

Sample Collection

Twenty-four submarine pillow basalts were dredged from the ocean floor along the CIR axis (16.7 °S to 20.6 °S), and the adjacent Gasitao, Three Magi, and Rodrigues ridges on our Knox11RR expedition (Füri *et al.*, 2008, 2011; Fig. S-1). In addition, several off-axis samples were collected along a perpendicularly offset lineament which extends westward from 66 °E to 64 °E toward the Mascarene Islands (*e.g.*, Réunion, Mauritius, Rodrigues islands; Parson *et al.*, 1993). Following the cruise, cumulate dunite xenoliths (n = 4) were collected from Piton Chisny on Réunion Island during a land-based field campaign.

Sample Preparation

Selected basalt samples were first ultrasonically cleaned in dichloromethane to remove any organic contaminants from the glass surface. Subsequently, approximately 300 mg of dried fresh glass, free of surficial alteration, phenocrysts, or large vesicles were handpicked using a binocular microscope. The selected glass was then ultrasonically cleaned in a 1:1 acetone-methanol mixture, dried, and transferred to the crushing apparatus.

Isotope Analyses

Neon and argon gases were released from basalts using a custom-built piston-activated *in vacuo* rock-crusher (see Hahm *et al.* (2012) for details). The released gas was purified using a dedicated cryogenic separation line whereby Ne and Ar were extracted and analysed individually. Neon and argon abundances and isotope ratios (as well as He abundances) were measured using a modified VG5440

mass spectrometer equipped with five Faraday cups and Daly photo-multiplier detector (Craig *et al.*, 1993; Hahm *et al.*, 2012), operated in peak jumping mode.

Neon results were corrected for procedural blanks and inferences of doubly-charged ^{40}Ar and CO_2 with ^{20}Ne and ^{22}Ne, respectively (see Niedermann *et al.* (1993) for details). ^{20}Ne procedural crusher blanks were $(15 \pm 8) \times 10^{-12}$ cm^3STP and ^{40}Ar procedural blanks were $(6 \pm 2) \times 10^{-9}$ cm^3STP, representing less than 10 % of sample yields.

Nitrogen was released using the same crushing mechanism described above for Ne-Ar; however, gases were purified on a separate vacuum clean-up line (see Barry *et al.* (2012) for details) prior to inlet into the VG5440 mass spectrometer, which was operated in static triple collection mode. Interfering CO species were monitored and CO corrections were applied to all samples. Procedural N_2 crusher blanks were $\sim 4.2 \pm 0.5 \times 10^{-6}$ cm^3STP on average, and were run prior to each sample analysis. Subsequent blank subtractions were applied, representing less than 20 % of the sample size. In addition, N_2/Ar ratios were measured separately, on an aliquot of the same gas, using a quadrupole mass spectrometer (QMS).

Atmospheric-derived Contamination

Different noble gas species in the mantle are variably affected by atmospheric-contamination – depending, in part, on their relative abundances in the mantle versus Earth's surface reservoirs. For example, Ne (18.2 ppm) and Ar (0.937 %) are enriched in the Earth's atmosphere relative to basaltic abundances and therefore basalts are highly susceptible to air-contamination processes. Air-like Ne-isotope contributions are ubiquitous in natural samples (Graham, 2002) with infiltration of air into basalts occurring through small micro-fractures, which can develop in glasses during seafloor sampling and/or handling in the laboratory (Ballentine and Barfod, 2000), and/or by assimilation of seawater-derived components (Farley and Craig, 1994).

Nitrogen is the most abundant (~78 %) gaseous species in the atmosphere; however, it occurs only in trace amounts in CIR basalts, and thus the potential for atmospheric contamination is substantial. Samples identified to be air-like with respect to Ne-Ar isotope systematics (Figs. S-2 and S-3) display non-air-like $\delta^{15}N$ and N_2/Ar values. In addition, the majority of CIR samples have N_2/Ar ratios well above the air value, indicating that air contamination is minimal. In Figure S-4, we plot $\delta^{15}N$ versus the air-normalised He/Ne values $(({}^{4}He/{}^{20}Ne)_{Sample}/({}^{4}He/{}^{20}Ne)_{Air})$ – a useful indicator of extent of air contamination. We show that both on-axis and off-axis CIR glasses have markedly (*i.e.* >2 orders of magnitude) higher $^{4}He/^{20}Ne$ ratios than air, and thus are not considered to be significantly modified by air-contributions.

Atmospheric Neon Correction

Although Ne-isotopes in basalts are highly susceptible to air-contamination, air-derived Ne contributions can be corrected by assuming that measured neon

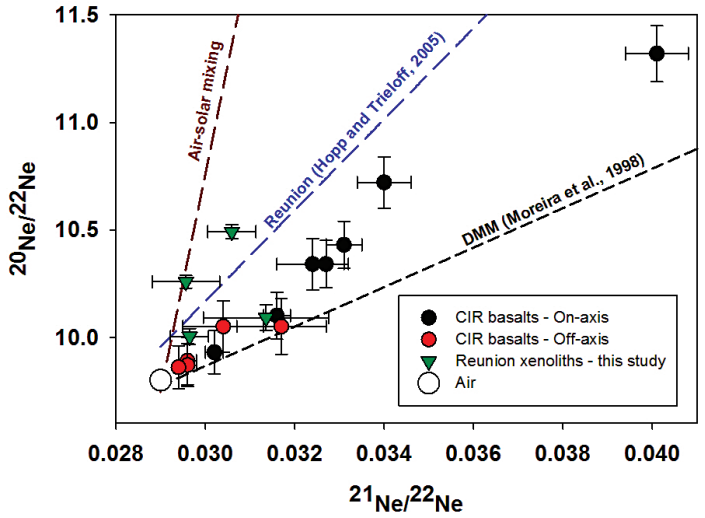

Figure S-2 Neon three-isotope plot ($^{20}Ne/^{22}Ne$ versus $^{21}Ne/^{22}Ne$) of CIR basaltic glasses and Réunion xenoliths. Three trend-lines are superimposed on the data: (1) the air-solar mixing line; (2) the Réunion line (Hopp and Trieloff, 2005); (3) the DMM (2[]D43) line (Moreira and Allègre, 1998). Uncertainties are at the 1σ level. Only samples with isotopes ratios >1 sigma from air are plotted.

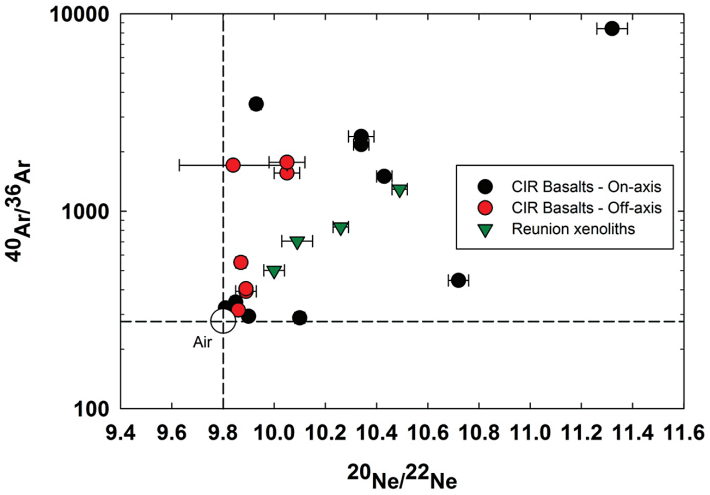

Figure S-3 Ar-isotopes versus Ne-isotopes. Ne-Ar systematics are coupled for the majority of samples, *i.e.* air-contamination and mantle isotope anomalies are evident in the same samples.

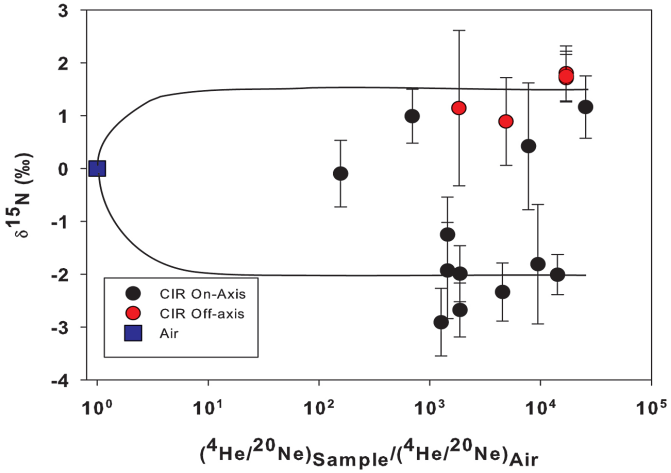

Figure S-4 N-isotopes ($\delta^{15}N$) versus air-normalised He/Ne values (= $^4He/^{20}Ne_S/^4He/^{20}Ne_A$). High He/Ne values relative to air (>100) suggest that all CIR basalt samples have undergone minimal air-contamination. Binary mixing trajectories are shown to postulated endmember values for 'plume = seds' ($\delta^{15}N$ = +1.5‰; $(^4He/^{20}Ne)_{Sample}/(^4He/^{20}Ne)_{Air} > 10^4$) and 'hybrid' ($\delta^{15}N$ = -2 ‰; $(^4He/^{20}Ne)_{Sample}/(^4He/^{20}Ne)_{Air} > 10^4$).

isotope values represent a binary mixture of atmospheric and mantle-derived neon. Following the methods of Honda *et al.* (1991), we extrapolate measured $^{20}Ne/^{22}Ne$ values to "solar" (*i.e.* Ne-B = 12.5) values in order to estimate air-corrected (*i.e.* $^{21}Ne/^{22}Ne_{EX}$) values. The following equations are used:

$$^{21}Ne/^{22}Ne_{EX} = (^{21}Ne/^{22}Ne_M - ^{21}Ne/^{22}Ne_A) / f22 + ^{21}Ne/^{22}Ne_A \quad \text{Eq. S-1}$$

where f22 is the proportion of mantle-derived Ne in a sample:

$$f22 = (^{20}Ne/^{22}Ne_M - ^{20}Ne/^{22}Ne_A) / (^{20}Ne/^{22}Ne_S - ^{20}Ne/^{22}Ne_A) \quad \text{Eq. S-2}$$

and $^{20}Ne/^{22}Ne_A$ and $^{21}Ne/^{22}Ne_A$ are the isotopic ratios of air, assumed to be 9.8 and 0.029, respectively, whereas $^{21}Ne/^{22}Ne_M$ is the measured sample $^{21}Ne/^{22}Ne$ value and $^{20}Ne/^{22}Ne_S$ is the assumed $^{21}Ne/^{22}Ne$ "solar" (*i.e.* Ne-B) neon component (=12.5; Trieloff *et al.*, 2000). Notably, the most air-like sample (*e.g.*, D3-1; highest ^{20}Ne content) cannot be corrected due to a $^{21}Ne/^{22}Ne_M$ value that is indistinguishable from air. The Ne–B endmember is obtained from gas-rich meteorites and lunar soils with a $^{20}Ne/^{22}Ne$ ratio of 12.52 ± 0.18, considered to represent implanted solar neon, now present within Earth's mantle (Black, 1972; Trieloff *et al.*, 2000, 2002; Ballentine *et al.*, 2005; Moreira, 2013). The primordial, "solar" neon component in Earth's mantle has also been assumed to be best represented by present-day solar wind (*i.e.* $^{20}Ne/^{22}Ne$ = 13.8; Benkert *et al.*, 1993; Kallenbach *et al.*, 1997); note, however, that selection of this endmember as opposed to Ne-B will not significantly affect the conclusions in the following discussion. Basalt CIR $^{21}Ne/^{22}Ne_{EX}$ values vary between 0.0437 ± 0.0009 and 0.0582 ± 0.0013 and fall

in the range of values observed in previous studies of plume-rift related systems (*e.g.*, Füri *et al.*, 2010; Hahm *et al.*, 2012). On-axis CIR $^{21}Ne/^{22}Ne_{EX}$ values range from 0.0437 ± 0.0011 to 0.0560 ± 0.0023, whereas off-axis samples range from 0.0441 ± 0.0017 to 0.0582 ± 0.0013.

Degassing Fractionation

In addition to air contamination, another process capable of modifying intrinsic mantle volatile features is degassing. Having discussed the importance of identifying air-contaminated samples and applying a correction when necessary, we now focus on additional processes which can modify source features, such as degassing. Degassing can potentially cause both isotope and relative abundance fractionation. For example, relative noble gas abundances (*e.g.*, $^{4}He/^{40}Ar^{*}$) can provide useful information about the mode and extent of volatile loss (Marty and Tolstikhin, 1998). Using this approach, an air-correction is first applied to the argon data by assuming that all ^{36}Ar is derived from the atmosphere. In this way the measured ^{40}Ar content in each sample can be corrected for the presence of atmospheric Ar to radiogenic Ar (*i.e.* $^{40}Ar^{*}$):

$$^{40}Ar^{*} = [^{36}Ar_{M}] \times [(^{40}Ar/^{36}Ar)_{M}\text{-}(^{40}Ar/^{36}Ar)_{A}] \qquad \text{Eq. S-3}$$

where $^{36}Ar_{M}$ and $(^{40}Ar/^{36}Ar)_{M}$ are the measured ^{36}Ar abundance and argon isotope ratio, respectively, and $(^{40}Ar/^{36}Ar)_{A}$ is the air ratio (= 298.56 ± 0.31; Lee *et al.*, 2006).

The measured He contents and calculated $^{40}Ar^{*}$, from Equation S-3, are then combined to give $^{4}He/^{40}Ar^{*}$ ratios, which can be used to determine the extent of degassing, as He is more soluble than Ar (S_{He}/S_{Ar} = 9.5; Jambon *et al.*, 1986; Lux, 1987) in basaltic magmas (Marty and Tolstikhin, 1998). Thus, residual (*i.e.* basalt) $^{4}He/^{40}Ar^{*}$ values should increase with increased degassing. Using estimates of upper mantle K/U (Arevalo *et al.*, 2009) and Th/U (O'Nions and McKenzie, 1993), a production ratio for $^{4}He/^{40}Ar^{*}$ of ~2 (Jambon *et al.*, 1986; Marty and Zimmermann, 1999) is assumed as a mantle starting value. In the case of the present sample suite, $^{4}He/^{40}Ar^{*}$ could not be calculated for two on-axis CIR basalt samples only (D1-1 and D3-1) due to measured air-like $^{40}Ar/^{36}Ar$ ratios (*i.e.* insignificant radiogenic ^{40}Ar contributions). Notably, all $^{4}He/^{40}Ar^{*}$ ratios calculated for CIR basalts are higher than the mantle production ratio of ~2 and range from 3.0 to 62, compared to Réunion xenoliths which fall between 1.3 and 2.0. In general, $^{4}He/^{40}Ar^{*}$ are low (<20), suggesting moderate but variable amounts of degassing. Two groups are evident: on axis samples, which have $^{4}He/^{40}Ar^{*}$ ratios <~10, with the exception of sample D2-1 ($^{4}He/^{40}Ar^{*}$ = 62) and off-axis samples, which have $^{4}He/^{40}Ar^{*}$ ratios >~10 with the exception of D26-2 ($^{4}He/^{40}Ar^{*}$ = 5.2). Higher $^{4}He/^{40}Ar^{*}$ ratios in off-axis samples (~5-10 x the production ratio) suggest more extensive degassing in off-axis portions of the crust, compared with on-axis samples. In contrast, $^{4}He/^{40}Ar^{*}$ values close to the mantle production value are measured in Réunion xenoliths, indicating that gas loss was insignificant or very minor.

In order to test if the observed N-isotope variations result from degassing-related modification, we plot $^{4}He/^{40}Ar^{*}$ versus $\delta^{15}N$ (Fig. 1d) and note that two

distinct (*i.e.* a positive and negative) fields are evident. Significantly, both fields have variable $^{4}He/^{40}Ar^{*}$, yet exhibit overlapping $\delta^{15}N$ values. For example, positive $\delta^{15}N$ samples have $^{4}He/^{40}Ar^{*}$ values that vary by a factor of 10, but all $\delta^{15}N$ values are indistinguishable within error. The same observation can be made for the negative $\delta^{15}N$ field where $^{4}He/^{40}Ar^{*}$ values range from 2 to 5: however, $\delta^{15}N$ values overlap. These results indicate that N-isotopes variations are independent of $^{4}He/^{40}Ar^{*}$ and thus we conclude that N-isotopes of CIR basalts have not experienced degassing-related fractionation. Significantly, this observation is consistent with previous compilation studies of various mid ocean ridge (MOR) and OIB settings (*e.g.*, Marty and Humbert, 1997; Fischer *et al.*, 2005), which also suggest that nitrogen isotope variations are independent of degassing. Therefore, nitrogen isotope variability in CIR basalts must be attributed to other processes – either mixing between isotopically distinct components in the mantle source and/or crustal contributions. In the following section, we investigate coupled He-Ne-Ar isotope systematics in order to assess if observed co-variations can be explained by mantle-mixing processes.

Solar Endmembers

Ne-isotope variations of CIR basalts suggest a solar component is present in the CIR mantle, with observed Ne-isotope variations best explained by mixing between DMM and primitive Réunion plume-like mantle endmembers (Fig. S-3). Assuming solar wind samples accurately approximate the proto-solar nebula (PSN; Marty *et al.*, 2011; Marty, 2012; Füri and Marty, 2015), there may also be a small, but detectable, primitive (*i.e.* solar) nitrogen component in the CIR mantle.

For a primordial starting neon component we choose here $^{21}Ne/^{22}Ne$ that is associated with solar wind implanted Ne–B ($^{20}Ne/^{22}Ne$ = 12.52 ± 0.18). Solar Ne–B as found in meteorites (Black, 1972) was long regarded as the actual solar composition, but Benkert *et al.* (1993) have shown that it is composed of low energetic solar wind particles ($^{20}Ne/^{22}Ne$ = 13.8 ± 0.1; $^{21}Ne/^{22}Ne$ = 0.0328 ± 0.0005) and a mass fractionated high energetic solar energetic particles (SEP) component ($^{20}Ne/^{22}Ne$ = 11.2 ± 0.2; $^{21}Ne/^{22}Ne$ = 0.0295 ± 0.0005), more deeply implanted and thus separable by stepwise etching of the carrier grains. We accordingly calculated $^{21}Ne/^{22}Ne$ of Ne–B as a mixture of these two subcomponents, yielding $^{21}Ne/^{22}Ne$ = 0.03118 ± 0.00048. This value is in agreement with, but more precise than, the value given by Black (1972) of $^{21}Ne/^{22}Ne$ = 0.0335 ± 0.0015.

He-Ne Isotope Variability

In Figure S-5, the air-corrected $^{21}Ne/^{22}Ne_{EX}$ values of CIR basalts as well as Réunion xenolith samples are plotted against He-isotopes, together with a series of binary mixing trajectories between postulated primordial (PRIM) and DMM end-members. Notably, $^{21}Ne/^{22}Ne_{EX}$ values in Réunion xenoliths range from 0.0325 ± 0.0108 to 0.0513 ± 0.0120, and fall in the range previously measured in Réunion lavas (Hanyu *et al.*, 2001; Trieloff *et al.*, 2002; Hopp and Trieloff, 2005).

The $^{21}Ne/^{22}Ne$ of PRIM (*i.e.* primitive solar component) is again assumed to be 0.03118 (Trieloff and Kunz, 2005) and the DMM $^{21}Ne/^{22}Ne$ endmember value is estimated to be 0.0594 by extrapolating the DMM trajectory (Sarda *et al.*, 1988) to the $^{20}Ne/^{22}Ne$ of Ne-B (= 12.5). In the case of He-isotopes, we assume a DMM endmember $^{4}He/^{3}He$ ratio of 90,000 (= 8 R_A) (Graham, 2002), and a primitive (PRIM) He-isotope endmember value of 280 R_A (Black, 1972; $^{4}He/^{3}He$ = 2580), consistent with the Ne-B component (*i.e.* both values were measured in gas-rich meteorite samples; Black, 1972). The curvature of binary mixing trajectories is controlled by the r-value = $(^{3}He/^{22}Ne)_{DMM}$ / $(^{3}He/^{22}Ne)_{PLUME}$. For reference, we also plot $^{21}Ne/^{22}Ne_{EX}$ versus $^{4}He/^{3}He$ data fields for previous studies of Réunion lavas (Hanyu *et al.*, 2001), and Iceland (Füri *et al.*, 2010), which represent the Réunion-plume component as well as an archetypal plume-MOR interaction.

The observed variations between Ne and He isotopes can be described by binary mixing between a primordial mantle endmember (PRIM) and a second endmember similar to DMM. However, unlike Ne-N relationships, CIR basalt and Réunion xenolith samples do not fall on a single Ne-He mixing curve, but rather require r-values between 0.4 and 30 to explain observed variations (Fig. S-5). Apart from one obvious outlier, on-axis CIR samples plot close to PRIM-DMM mixing curves with r-values between 1 and 30, whereas the majority of off-axis samples fall between 1 and 5, with one outlier with an r-value of 30. The fact that all basalt samples require r-values greater than unity, implies a higher $^{3}He/^{22}Ne$ ratio of the DMM endmember compared to the $^{3}He/^{22}Ne$ ratio of the primordial mantle component (*i.e.* $(^{3}He/^{22}Ne)_{DMM} > (^{3}He/^{22}Ne)_{PRIM}$).

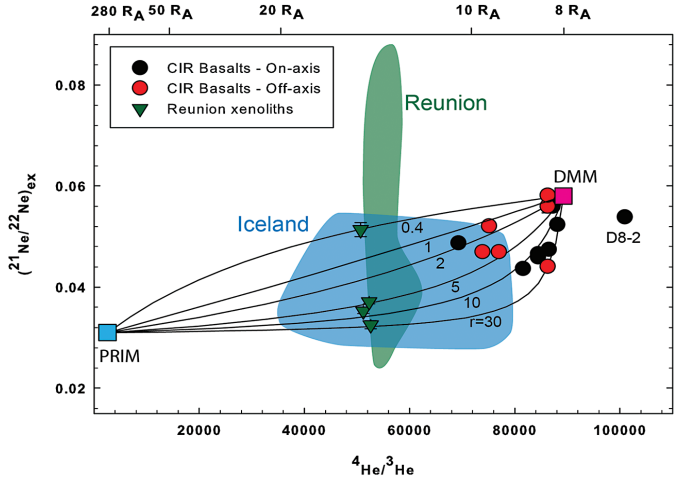

Figure S-5 $(^{21}Ne/^{22}Ne)_{EX}$ (*i.e.* air-corrected $^{21}Ne/^{22}Ne$ values) versus $^{4}He/^{3}He$ values of CIR basalts and Réunion xenoliths, plotted together with binary mixing curves between a primordial mantle endmember (PRIM) and a DMM-like component. The curvature of the hyperbolic mixing lines is described by r = $(^{3}He/^{22}Ne)_{DMM}/(^{3}He/^{22}Ne)_{PRIM}$. In addition, data fields are shown for Réunion lavas (Hanyu *et al.*, 2001) and Iceland subglacial basalts (Füri *et al.*, 2010).

If we assume that the DMM endmember $^{3}He/^{22}Ne$ ratio is constant throughout the CIR, then lower r-values in off-axis samples suggest a higher relative PRIM $^{3}He/^{22}Ne$ endmember in the plume source. In this regard, CIR basalts resemble other plume-related glasses (*e.g.*, Iceland; Füri *et al.*, 2010). Significantly, all Réunion xenolith samples plot closer to the PRIM endmember compared with CIR basalt samples and overlap with Réunion lavas (Hanyu *et al.*, 2001), consistent with a higher $^{3}He/^{22}Ne$ plume contribution in the admixture. Notably, mixing trajectories for xenolith samples span the entire range observed in CIR basalts (*i.e.* r-values between ~0.4 and 30), however, this range is bracketed by Réunion lava samples (Hanyu *et al.*, 2001), which span an even broader range (Fig. S-5). The single outlying on-axis basalt sample (Fig. S-2; D8-2) falls outside the mixing envelope defined by the series of binary mixing curves between PRIM and DMM endmembers; D8-2 is marked by lower than DMM He-isotopes and thus an additional endmember (with low $^{3}He/^{4}He$) is required to account for the He–Ne systematics; radiogenic He (accompanied by insignificant nucleogenic Ne) produced within the crust is a distinct possibility. This observation in agreement with the conclusions of Füri *et al.* (2011), who explained low He-isotope (*i.e.* $^{3}He/^{4}He$ < DMM) samples observed in the ~18.1 °S portion of the CIR by closed system radiogenic ^{4}He in-growth in a "fossil" Réunion mantle component. Furthermore, this finding is consistent with larger contributions from the Réunion-like (*i.e.* plume) component, which were identified in the Ne-N isotope systematics of sample D8-2.

An alternative explanation for variations in $^{21}Ne/^{22}Ne_{ex}$ values between presumed upper and lower mantle reservoirs is elemental He/Ne heterogeneities in the mantle. For example, Moreira *et al.* (2001) proposed that different mantle reservoirs (*i.e.* DMM versus PRIM) could have evolved from the same He and Ne isotope compositions but with distinct $^{3}He/^{22}Ne$ ratios and that subsequent ingrowth of nucleogenic ^{21}Ne and radiogenic ^{4}He have produced the observed range in $^{21}Ne/^{22}Ne_{ex}$ and $^{3}He/^{4}He$ values. Nucleogenic ^{21}Ne is generated by the ^{18}O (α,n) ^{21}Ne and ^{24}Mg (n,α) ^{21}Ne reactions (Wetherill, 1954), resulting in an increase in the $^{21}Ne/^{22}Ne$ ratio and $\delta^{21}Ne$ values over time. Since α-particles are derived from U and Th decay, the production of radiogenic ^{4}He and nucleogenic ^{21}Ne ($^{21}Ne^{*}$) should therefore be directly coupled, and high $^{4}He/^{3}He$ (*i.e.* low $^{3}He/^{4}He$) ratios would therefore correlate with high $^{21}Ne/^{22}Ne_{EX}$ values. However, in CIR basalts and Réunion xenoliths, measured $^{3}He/^{22}Ne$ ratios vary over 2 orders of magnitude (0.02 to 3.93). If mantle heterogeneities were the origin of these variations it would imply that the $^{3}He/^{22}Ne$ ratio in the mantle source varied by a factor of ~200. However, there is no known mechanism that can preserve such large $^{3}He/^{22}Ne$ disparities within a single mantle domain for such long durations (*i.e.* over Earth history). Therefore, we propose that the He–Ne characteristics of CIR basalt and Réunion xenolith samples are better explained by the binary mixing scenario presented in Figure S-5.

Table S-1 Mantle regassing sensitivity to various input parameters.

Study[a]	DMM End member $\delta^{15}N$ (‰)	PLM End member $\delta^{15}N$ (‰)	Initial Mantle End member $\delta^{15}N$ (‰)[b]	Starting [N] of mantle (ppm)[c]	Onset of subduction (Ga)[d]	Regassing Flux (F_{DMM}) ($\times10^9$mol/yr)	Regassing Flux (F_{PLM}) ($\times10^9$mol/yr)	F_{PLM}/F_{DMM}
This study	**-2.1**	**1.3**	*-40*	*0.27*	*1.1*	16.7	53.3	3.2
			-40	*0.27*	*2.5*	9.4	24.2	2.6
			-40	*0.27*	*3.9*	7.3	15.8	2.2
			-40	*36*	*1.1*	1767	7106	4
			-40	*36*	*2.5*	781	3133	4
			-40	*36*	*3.9*	517	2071	4
			-383	*0.27*	*1.1*	19.7	58.3	3
			-383	*0.27*	*2.5*	11	26.2	2.4
			-383	*0.27*	*3.9*	8.6	17.5	2
			-383	*36*	*1.1*	2065	7653	3.7
			-383	*36*	*2.5*	911	3376	3.7
			-383	*36*	*3.9*	601	2229	3.7
Johnson and Goldblatt, 2015	**-1.1**	**2.5**	*-40*	*0.27*	*1.1*	16.8	54.2	3.2
			-40	*0.27*	*2.5*	9.4	24.1	2.6
			-40	*0.27*	*3.9*	7.5	16.2	2.1
			-40	*36*	*1.1*	1815	7317	4
			-40	*36*	*2.5*	801	3222	4
			-40	*36*	*3.9*	529	2124	4
			-383	*0.27*	*1.1*	19.7	58.3	3
			-383	*0.27*	*2.5*	11	26.3	2.4
			-383	*0.27*	*3.9*	8.7	17.4	2
			-383	*36*	*1.1*	2074	7726	3.7
			-383	*36*	*2.5*	914	3402	3.7
			-383	*36*	*3.9*	602	2244	3.7
Dauphas and Marty, 1999	**-4**	**3**	*-40*	*0.27*	*1.1*	16	56.5	3.5
			-40	*0.27*	*2.5*	8.9	25.1	2.8
			-40	*0.27*	*3.9*	7	16.4	2.3
			-40	*36*	*1.1*	1684	7416	4.4
			-40	*36*	*2.5*	744	3269	4.4
			-40	*36*	*3.9*	491	2152	4.4
			-383	*0.27*	*1.1*	19.5	58.5	3
			-383	*0.27*	*2.5*	10.9	26.1	2.4
			-383	*0.27*	*3.9*	8.5	17	2
			-383	*36*	*1.1*	2061	7739	3.7
			-383	*36*	*2.5*	905	3392	3.7
			-383	*36*	*3.9*	596	2229	3.7

[a] The average N-isotope values for the modern DMM and PLM (*e.g.*, OIB-source) mantle source regions from these studies are used.
[b] Initial mantle $\delta^{15}N$ endmember values of -40 ‰ and -383 ‰ are from Cartigny and Marty (2013) and Marty *et al.* (2011), respectively.
[c] Initial mantle [N] endmember contents of 0.27 ppm and 36 ppm are from Marty (2012) and Cartigny and Marty (2013), respectively.
[d] Onset of subduction estimates of 1.1 Ga, 2.5 Ga and 3.9 Ga are based on Cartigny and Marty (2013), Kusky *et al.* (2001) and Condie and Pease (2008), respectively.
Values in italics are assumptions, remaining values are model output.

Supplementary Information References

Arevalo, R., McDonough, W.F., Luong, M. (2009) The K/U ratio of the silicate Earth: Insights into mantle composition, structure and thermal evolution. *Earth and Planetary Science Letters* 278, 361-369.

Ballentine, C.J., Barfod, D.N. (2000) The origin of air-like noble gases in MORB and OIB. *Earth and Planetary Science Letters* 180, 39–48.

Ballentine, C.J., Marty, B., Lollar, B.S., Cassidy, M. (2005) Neon isotopes constrain convection and volatile origin in the Earth's mantle. *Nature* 433, 33–38.

Barry, P.H., Hilton, D.R., Halldórsson, S.A., Hahm, D., Marti, K. (2012) High precision nitrogen isotope measurements in oceanic basalts using a static triple collection noble gas mass spectrometer. *Geochemistry Geophysics Geosystems* 13, Q01019.

Bebout, G.E., Lazzeri, K.E., Geiger, C.A. (2016) Pathways for nitrogen cycling in Earth's crust and upper mantle: A review and new results for microporous beryl and cordierite. *American Mineralogist* 101, 7-24.

Benkert, J.P., Baur, H., Signer, P., Wieler, R. (1993) He, Ne, and Ar from the solar-wind and solar energetic particles in lunar ilmenites and pyroxenes. *Journal of Geophysical Research – Planets* 98, 13147–13162.

Black, D.C. (1972) On the origins of trapped helium, neon and argon isotopic variations in meteorites – I. Gas-rich meteorites, lunar soil and breccia. *Geochimica et Cosmochimica Acta* 36, 347–375.

Busigny, V., Lebeau, O., Ader, M., Krapez, B., Bekker, A. (2013) Nitrogen cycle in a Late Archean ferruginous ocean. *Chemical Geology* 362, 115-130.

Cartigny, P., Marty, B. (2013) Nitrogen isotopes and mantle geodynamics: The emergence of life and the atmosphere–crust–mantle connection. *Elements* 9, 359-366.

Cartigny, P., Harris, J.W., Phillips, D., Girard, M., Javoy M. (1998) Subduction-related diamonds? The evidence for a mantle-derived origin from coupled $\delta^{13}C$ - $\delta^{15}N$ determinations. *Chemical Geology* 147, 147-159.

Cartigny, P., Jendrzejewski, N., Pineau, F., Petit, E., Javoy, M. (2001) Volatile (C, N, Ar) variability in MORB and the respective roles of mantle source heterogeneity and degassing: the case of the Southwest Indian Ridge. *Earth and Planetary Science Letters* 194, 241–257.

Condie, K.C., Pease, V. (2008) When did plate tectonics begin on planet Earth? Geological Society of America Special Paper 440, Boulder Colorado, USA.

Courtillot, V., Davaille, A., Besse, J., Stock, J. (2003) Three distinct types of hotspots in the Earth's mantle. *Earth and Planetary Science Letters* 205(3), 295-308.

Craig, H., Marti, K., Wiens, R. (1993) A Static Mass Spectrometer With Triple Collection for Nitrogen and Neon Isotopes. SIO Reference Series. Scripps Institute of Oceanography, La Jolla, California, USA, 93-11, 1–20A.

Dauphas, N., Marty, B. (1999) Heavy nitrogen in carbonatites of the Kola Peninsula: A possible signature of the deep mantle. *Science* 286, 2488-2490.

Duncan, R.A., Backman, J., Peterson, L., Shipboard Scientific Party (1989) Réunion hotspot activitity through tertiary time: Initial results from the ocean drilling program, leg 115. *Journal of Volcanology and Geothermal Research* 36, 193-198.

Duncan, R.A., Backman, J., Peterson, L. (1990) The volcanic record of the Réunion hot spot. *Proceedings of the Ocean Drilling Program Scientific Results* 115, 3–10.

Dyment, J., Gallet, Y., Magofond 2 Scientific Party (1999) The Magofond 2 cruise: A surface and deep tow survey on the past and present Central Indian Ridge. *InterRidge News* 8, 25–31.

Dyment, J., Hémond, C., Gimnaut Scientific Party (2000) Deep-sea exploration of the Central Indian Ridge at 19°S. *InterRidge News* 9, 29–32.

Farley, K.A., Craig, H. (1994) Atmospheric argon contamination of ocean island basalt olivine phenocrysts. *Geochimica et Cosmochimica Acta* 58, 2509–2517.

Fischer, T.P., Hilton, D.R., Zimmer, M.M., Shaw, A.M., Sharp, Z.D., Walker, J.A. (2002) Subduction and recycling of nitrogen along the Central American margin. *Science* 297, 1154-1157.

Fischer, T.P., Takahata, N., Sano, Y., Sumino, H., Hilton, D.R. (2005) Nitrogen isotopes of the mantle: Insights from mineral separates. *Geophysical Research Letters* 32, L11305.

Fretzdorff, S., Haase, K.M. (2002) Geochemistry and petrology of lavas from the submarine flanks of Réunion Island (western Indian Ocean): implications for magma genesis and the mantle source. *Mineralogy and Petrology* 75, 153-184.

Füri, E., Marty, B. (2015) Nitrogen isotope variations in the Solar System. *Nature Geoscience* 8, 515-522.

Füri, E., Hilton, D.R., KNOX11RR Scientific Party (2008) Sampling and surveying ridge-hot spot interaction on the Central Indian Ridge, 19°S: Cruise KNOX11RR. *InterRidge News* 17, 28–29.

Füri, E., Hilton, D.R., Halldórsson, S.A., Barry, P.H., Hahm, D., Fischer, T.P., Gronvold, K. (2010) Apparent decoupling of the He and Ne isotope systematics of the Icelandic mantle: the role of He depletion, melt mixing, degassing fractionation and air interaction. *Geochimica et Cosmochimica Acta* 74, 3307–3332.

Füri, E., Hilton, D.R., Murton, B.J., Hemond, C., Dyment, J., Day, J. M. D. (2011) Helium isotope variations between Réunion Island and the Central Indian Ridge (17°-21°S): new evidence for ridge-hotspot interaction. *Journal of Geophysical Research – Solid Earth* 116, B02207.

Gillot, P.Y., Nativel, P. (1989) Eruptive history of the Piton de la Fournaise volcano, Réunion, Indian Ocean. *Journal of Volcanology and Geothermal Research* 36, 53–65.

Graham, D.W. (2002) Noble gas isotope geochemistry of mid–ocean ridge and ocean island basalts: Characterization of mantle source reservoirs. *RIMS* 47, 247–317.

Hahm, D., Hilton, D.R., Castillo, P.R., Hawkins, J.W., Hanan, B.B., Hauri, E.H. (2012) An overview of the volatile systematics of the Lau Basin – Resolving the effects of source variation, magmatic degassing and crustal contamination. *Geochimica et Cosmochimica Acta* 85, 88-113.

Halama, R., Bebout, G.E., John, T., Schenk, V. (2010). Nitrogen recycling in subducted oceanic lithosphere: The record in high-and ultrahigh-pressure metabasaltic rocks. *Geochimica et Cosmochimica Acta* 74, 1636-1652.

Halama, R., Bebout, G.E., John, T., Scambelluri, M. (2014). Nitrogen recycling in subducted mantle rocks and implications for the global nitrogen cycle. *International Journal of Earth Sciences* 103, 2081-2099.

Hanyu, T., Dunai, T.J., Davies, G.R., Kaneoka, I., Nohda, S., Uto, K. (2001) Noble gas study of the Reunion hot spot: evidence for distinct less-degassed mantle sources. *Earth and Planetary Science Letters* 193, 83–98.

Hilton, D.R., Fischer, T.P., Marty, B. (2002) Noble gases and volatile recycling at subduction zones. In: Porcelli, D., Ballentine, C.J., Wieler, R. (Eds.) Noble Gases in Cosmochemistry and Geochemistry. *Mineralogical Society of America* 47 319-370.

Hofmann, A.W., White, W.M. (1982) Mantle plumes from ancient oceanic crust. *Earth and Planetary Science Letters* 57, 421-436.

Holland, G., Ballentine, C.J. (2006) Seawater subduction controls the heavy noble gas composition of the mantle. *Nature* 441, 186-191.

Honda, M., Woodhead, J.D. (2005). A primordial solar-neon enriched component in the source of EM-I-type ocean island basalts from the Pitcairn Seamounts, Polynesia. *Earth and Planetary Science Letters* 236, 597-612.

Honda, M., McDougall, I., Patterson, D.B., Doulgeris, A., Clague, D.A. (1991) Possible solar noble-gas component in Hawaiian basalts. *Nature* 349, 149 – 151.

Hopp, J., Trieloff, M. (2005) Refining the noble gas record of the Réunion mantle plume source: Implications on mantle geochemistry. *Earth and Planetary Science Letters* 240, 573–588.

Hopp, J., Ionov, D.A. (2011) Tracing partial melting and subduction-related metasomatism in the Kamchatkan mantle wedge using noble gas compositions. *Earth and Planetary Science Letters* 302, 121–131.

Jackson, C.R.M., Parman, S., Kelley, S.P., Cooper, R.F. (2013a) Noble gas transport into the mantle facilitated by high solubility in amphibole. *Nature Geoscience* 6, 562–565.

Jackson, C.R.M., Parman, S.W., Kelley, S.P., Cooper, R.F. (2013b) Constraints on light noble gas partitioning at the conditions of spinel-peridotite melting. *Earth and Planetary Science Letters* 384, 178–187.

Jackson, C.R.M., Parman, S.W., Kelley, S.P., Cooper, R.F. (2015) Light noble gas dissolution into ring structure-bearing materials and lattice influences on noble gas recycling. *Geochimica et Cosmochimica Acta* 159, 1–15.

Jackson, C.R.M., Shuster, D.L., Parman, S.W., Smye, A.J. (2016). Noble gas diffusivity hindered by low energy sites in amphibole. *Geochimica et Cosmochimica Acta* 172, 65-75.

Jambon, A., Weber, H.W., Braun, O. (1986) Solubility of He, Ne, Ar, Kr and Xe in a basalt melt in the range 1250–1600°C - Geochemical implications. *Geochimica et Cosmochimica Acta* 50, 401–408.

Javoy, M., Pineau, F., Delorme, H. (1986) Carbon and nitrogen isotopes in the mantle. *Chemical Geology* 57, 41–62.

Johnson, B., Goldblatt, C. (2015) The nitrogen budget of Earth. *Earth-Science Reviews* 148, 150-173.

Kallenbach, R., Ipavich, F.M., Bochsler, P., Hefti, S., Hovestadt, D., Grünwaldt, H., Hilchenbach, M., Axford, W.I., Balsiger, H., Bürgi, A., Coplan, M.A., Galvin, A.B., Geiss, J., Gliem, F., Gloeckler, G., Hsieh, K.C., Klecker, B., Lee, M.A., Livi, S., Managadze, G.G., Marsch, E., Möbius, E., Neugebauer, M., Reiche, K.U., Scholer,

M., Verigin, M.I., Wilken, B. Wurz, P. (1997) Isotopic composition of solar wind neon measured by CELIAS/MTOF on board SOHO. *Journal of Geophysical Research – Space* 102, 26895–26904.

Kendrick, M.A., Scambelluri, M., Honda, M., Phillips, D. (2011). High abundances of noble gas and chlorine delivered to the mantle by serpentinite subduction. *Nature Geoscience* 4, 807-812.

Kendrick, M.A., Honda, M., Pettke, T., Scambelluri, M., Phillips, D., Giuliani, A. (2013) Subduction zone fluxes of halogens and noble gases in seafloor and forearc serpentinites. *Earth and Planetary Science Letters* 365, 86–96.

Kusky, T.M., Li, J.H., Tucker, R.D. (2001) The Archean Dongwanzi ophiolite complex, North China Craton: 2.505-billion-year-old oceanic crust and mantle. *Science* 292, 1142-1145.

Li, Y., Keppler, H. (2014) Nitrogen speciation in mantle and crustal fluids. *Geochimica et Cosmochimica Acta* 129, 13-32.

Li, L., Bebout, G.E., Idleman, B.D. (2007) Nitrogen concentration and δ 15 N of altered oceanic crust obtained on ODP Legs 129 and 185: insights into alteration-related nitrogen enrichment and the nitrogen subduction budget. *Geochimica et Cosmochimica Acta* 71, 2344-2360.

Li, Y., Wiedenbeck, M., Shcheka, S., Keppler, H. (2013). Nitrogen solubility in upper mantle minerals. *Earth and Planetary Science Letters* 377, 311-323.

Lux, G. (1987) The behavior of noble gases in silicate liquids: solution, diffusion, bubbles and surface effects, with applications to natural samples. *Geochimica et Cosmochimica Acta* 51, 1549–1560.

Mahoney, J.J., Natland, J.H., White, W.M., Poreda, R., Bloomer, S.H., Baxter, A.N. (1989) Isotopic and geochemical provinces of the Western Indian Ocean spreading centers. *Journal of Geophysical Research* 94, 4033–4052.

Marty, B. (2012) The origins and concentrations of water, carbon, nitrogen and noble gases on Earth. *Earth and Planetary Science Letters* 313-314, 56-66.

Marty, B., Humbert, F. (1997) Nitrogen and argon isotopes in oceanic basalts. *Earth and Planetary Science Letters* 152, 101-112.

Marty, B., Tolstikhin, I.N. (1998) CO_2 fluxes from mid-ocean ridges, arc and plumes. *Chemical Geology* 145, 233–248.

Marty, B., Zimmermann, L. (1999) Volatiles (He, C, N, Ar) in mid-ocean ridge basalts: assessment of shallow-level fractionation and characterization of source composition. *Geochimica et Cosmochimica Acta* 63, 3619–3633.

Marty, B., Dauphas, N. (2003) The nitrogen record of crust-mantle interaction and mantle convection from Archean to present. *Earth and Planetary Science Letters* 206, 397– 410.

Marty, B., Chaussidon, M., Jurewicz, A.,Wiens, R., Burnett, D.S. (2011) A ^{15}N-poor isotopic composition for the solar system as shown by Genesis solar wind samples. *Science* 332, 1533–1536.

Matsumoto, T., Chen, Y., Matsuda, J.I. (2001) Concomitant occurrence of primordial and recycled noble gases in the Earth's mantle. *Earth and Planetary Science Letters* 185, 35–47.

McDougall, I., Upton, B.G.J., Wadsworth, W.J. (1965) A geological reconnaissance of Rodriguez Island Indian Ocean. *Nature* 206, 26–27.

Mikhail, S., Sverjensky, D.A. (2014) Nitrogen speciation in upper mantle fluids and the origin of Earth's nitrogen-rich atmosphere. *Nature Geoscience* 7, 816-819.

Mitchell, E.C., Fischer, T.P., Hilton, D.R., Hauri, E.H., Shaw, A.M., de Moor, J.M., Sharp, Z.D., Kazahaya, K. (2010) Nitrogen sources and recycling at subduction zones: Insights from the Izu-Bonin-Mariana arc. *Geochemistry, Geophysics, Geosystems* 11, 2.

Mohapatra, R.K., Murty, S.V.S. (2002) Nitrogen and noble gas isotopes in mafic and ultramafic inclusions in the alkali basalts from Kutch and Reunion—implications for their mantle sources. *Journal of Asian Earth Sciences* 20, 867-877.

Moreira, M. (2013) Noble gas constraints on the origin and evolution of Earth's volatiles. *Geochemical Perspectives* 2, 229-230.

Moreira, M., Allègre, C.J. (1998) Helium-neon systematics and the structure of the mantle. *Chemical Geology* 147, 53–59.

Moreira, M., Breddam, K., Curtice, J., Kurz, M.D. (2001) Solar neon in the Icelandic mantle: new evidence for an undegassed lower mantle. *Earth and Planetary Science Letters* 185, 15–23.

Morgan, W.J. (1978) Rodriguez, Darwin, Amsterdam, a second type of hot spot island. *Journal of Geophysical Research* 83, 5355–5360.

Morgan, W.J. (1981) Hot spot tracks and the opening of the Atlantic and Indian oceans. *In The Sea* 7, 443–487.

Mukhopadhyay, S. (2012) Early differentiation and volatile accretion recorded in deep-mantle neon and xenon. *Nature* 486, 101–104.

Murton, B.J., Tindle, A.G., Milton, J.A., Sauter, D. (2005) Heterogeneity in southern Central Indian Ridge MORB: implications for ridge– hot spot interaction. *Geochemistry Geophysics Geosystems* 6, Q03E20.

Nagao, K., Takahashi, E. (1993) Noble gases in the mantle wedge and lower crust: an inference from the isotopic analyses of xenoliths from Oki-Dogo and Ichinomegata, Japan. *Geochemical Journal* 27, 229–240.

Nauret, F., Abouchami, W., Galer, S.J.G., Hofmann, A.W., Hémond, C., Chauvel, C., Dyment, J. (2006) Correlated trace element - Pb isotope enrichments in Indian MORB along 18–20°S, Central Indian Ridge. *Earth and Planetary Science Letters* 245, 137–152.

Niedermann, S., Graf, T., Marti, K. (1993) Mass spectrometric identification of cosmic-ray-produced neon in terrestrial rocks with multiple neon components. *Earth and Planetary Science Letters* 118, 65–73.

Okino, K., Ichikawa, Y., Tamaki, T. (2008) Detailed morphology of the Central Indian Ridge between 20°15S and 15°30S: Implication for hot spot ridge interaction. Proceedings of the Japan Geoscience Union (JPGU), Chiba, Japan, Abstract J164 002.

O'Nions, R.K., McKenzie, D. (1993) Estimates of mantle thorium/uranium ratios from Th, U and Pb isotope abundances in basaltic melts. *Philosophical Transactions of the Royal Society* 342, 65–77.

Palot, M., Cartigny, P., Harris, J.W., Kaminsky, F.V., Stachel, T. (2012) Evidence for deep mantle convection and primordial heterogeneity from nitrogen and carbon stable isotopes in diamond. *Earth and Planetary Science Letters* 357, 179-193.

Parai, R., Mukhopadhyay, S. (2015) The evolution of MORB and plume mantle volatile budgets: constraints from fission Xe isotopes in Southwest Indian Ridge basalts. *Geochemistry Geophysics Geosystems* 16, 719–735.

Parai, R., Mukhopadhyay, S., Standish, J. (2012) Heterogeneous upper mantle Ne, Ar and Xe isotopic compositions and a possible Dupal noble gas signature recorded in basalts from the Southwest Indian Ridge. *Earth and Planetary Science Letters* 359, 227–239.

Parson, L.M., Patriat, P., Searle, R.C., Briais, A.R. (1993). Segmentation of the Central Indian Ridge between 12 12' S and the Indian Ocean triple junction. *Marine Geophysical Researches* 15, 265-282.

Paul, D., White, W.M., Blichert-Toft, J. (2005) Geochemistry of Mauritius and the origin of rejuvenescent volcanism on oceanic island volcanoes. *Geochemistry Geophysics Geosystems* 6, Q06007.

Pető, M.K., Mukhopadhyay, S., Kelley, K.A. (2013). Heterogeneities from the first 100 million years recorded in deep mantle noble gases from the Northern Lau Back-arc Basin. *Earth and Planetary Science Letters* 369, 13-23.

Sano, Y., Takahata, N., Nishio, Y., Marty, B. (1998) Nitrogen recycling in subduction zones. *Geophysical Research Letters 25*, 2289-2292.

SARDA, P. (2004) Surface noble gas recycling to the terrestrial mantle. *Earth and Planetary Science Letters* 228, 49-63.

SARDA, P., STAUDACHER, T., ALLÈGRE, C.J. (1988) Neon isotopes in submarine basalts. *Earth and Planetary Science Letters* 91, 73-88.

SMITH, W.H.F., SANDWELL, D.T. (1997) Global sea floor topography from satellite altimetry and ship depth soundings. *Science* 277, 1956-1962.

STAUDACHER, T., ALLÈGRE, C.J. (1988) Recycling of oceanic crust and sediments: the noble gas subduction barrier. *Earth and Planetary Science Letters* 89, 173-183.

SUMINO, H., BURGESS, R., MIZUKAMI, T., WALLIS, S.R., HOLLAND, G., BALLENTINE, C.J. (2010) Seawater-derived noble gases and halogens preserved in exhumed mantle wedge peridotite. *Earth and Planetary Science Letters* 294, 163-172.

THOMAZO, C., PAPINEAU, D. (2013) Biogeochemical cycling of nitrogen on the early Earth. *Elements* 9, 345-351.

TRIELOFF, M., KUNZ, J. (2005) Isotope systematics of noble gases in the Earth's mantle: possible sources of primordial isotopes and implications for mantle structure. *Physics of the Earth and Planetary Interiors* 148, 13-38.

TRIELOFF, M., KUNZ, J., CLAGUE, D.A., HARRISON, D., ALLÈGRE, C.J. (2000) The nature of pristine noble gases in mantle plumes. *Science* 288, 1036–1038.

TRIELOFF, M., KUNZ, J., ALLÈGRE C.J. (2002) Noble gas systematics of the Réunion mantle plume source and the origin of primordial noble gases in Earth's mantle. *Earth and Planetary Science Letters* 200, 297–313.

TUCKER, J.M., MUKHOPADHYAY, S., SCHILLING, J.G. (2012) The heavy noble gas composition of the depleted MORB mantle (DMM) and its implications for the preservation of heterogeneities in the mantle. *Earth and Planetary Science Letters* 355, 244-254.

ULRICH, M., HEMOND, C., NONNOTTE, P., JOCHUM, K.P. (2012) OIB/seamount recycling as a possible process for E-MORB genesis. *Geochemistry Geophysics Geosyst*ems 13, Q0AC19.

WATENPHUL, A., WUNDER, B., WIRTH, R., HEINRICH, W. (2010) Ammonium-bearing clinopyroxene: a potential nitrogen reservoir in the Earth's mantle. *Chemical Geology* 270, 240-248.